Supplementary Information (SI) for Journal of Materials Chemistry B.
This journal is © The Royal Society of Chemistry 2026

SUPPORTING INFORMATION

MATERIALS

Amino acids (γ-benzyl-l-glutamate, and O-benzyl-l-tyrosine) and triphosgene were obtained from ChemImpex and used without further purification for the N-carboxyanhydride (NCA) synthesis. Solvents for synthesis (tetrahydrofuran, dimethylformamide) diethyl ether, hexanes, and glacial acetic acid were obtained from Fisher Chemical. Tetrahydrofuran (THF) and dimethylformamide (DMF) were dried via solvent still, degassed with dry N_2, and passed through a column of activated neutral alumina before use. Hexylamine was obtained from Aldrich. Hydrobromic acid (48% w/w aqueous) was obtained from Alfa Aesar. Acetic acid (glacial) was purchased from Fisher Chemical. Trifluoroacetic acid was obtained from EMD Millipore. Deuterated solvents for NMR (DMSO-d6 and TFA-d) were purchased from Cambridge Isotopes.

Simulated gastric fluid (SGF) was prepared according to United States Pharmacopeia (USP) guidelines. 2.0 g of NaCl was dissolved in 7.0 mL of concentrated HCl and 800 mL of deionized water, the pH of the solution was adjusted to 1.2 using 0.1 M NaOH and 0.1 M HCl, and the solution was quantitatively transferred to a 1000 mL volumetric flask and diluted to the mark with deionized water. Simulated intestinal fluid (SIF) was prepared according to USP guidelines. 6.8 g of KH2PO4 and 0.896 g of NaOH were dissolved in 800 mL of deionized water, the pH of the solution was adjusted to 6.8 using 0.1 M NaOH or 0.1 M H_3PO_4, and the solution was quantitatively transferred to a 1000 mL volumetric flask and diluted to the mark with deionized water. An Accumet Basic AB15 pH meter (Fisher Scientific, Waltham, MA) was used for all pH adjustments. SGF with pepsin (5.34 U/mL) was prepared by adding 3.2 g of pepsin per liter of SGF, according to USP guidelines. SIF with trypsin (100 U/mL) and chymotrypsin

(25 U/mL) was prepared according to literature precedent. Pepsin was purchased from VWR, trypsin was purchased from VWR, and alpha-chymotrypsin was purchased from MP Biomedicals.

All cell culture reagents were acquired from ThermoFisher Scientific. RAW 264.7 murine macrophages and NIH 3T3 fibroblasts were cultured in Dulbecco's Modified Eagle Medium with 4500 mg/L d-glucose, 584 mg/L L-glutamine, and 100 mg/L sodium pyruvate (catalog #11995065). This basal media was supplemented with 10% v/v fetal bovine serum (catalog #26140079) and penicillin streptomycin antibiotics (catalog #15140122) that was diluted to a final concentration of 100 U/mL. The cells were cultured in an incubator at 37 °C with a humidified atmosphere at 5% CO2.

CHARACTERIZATION

Fourier transform infrared spectroscopy (FTIR).

FTIR attenuated total reflectance spectroscopy was performed using a PerkinElmer Frontier FTIR spectrometer with a germanium crystal. Spectra were acquired with a 1 cm^{-1} resolution over a range of 700–4000 cm^{-1}. Using the Spectrum software (PerkinElmer), spectra were corrected for attenuated total reflectance mode, baseline corrected, and converted to absorbance.

Confocal microscopy.

Polypeptide suspensions were prepared with a concentration of 1 mg/mL in SIF. Microscope images of the adsorbent particles were acquired in petri dishes (Corning, 100x10 mm) on an EVOS® FL Auto Cell Imaging System (ThermoFisher Scientific) with a 10X and 20X 0.30 numerical aperture objectives in transmission mode.

Scanning electron microscopy (SEM).

A Quanta 600 FEG scanning electron microscope was used to determine the surface morphology of the polypeptides. Freeze-dried polypeptide powders were applied to carbon tape and coated with 3 nm of platinum using the EMS Q300T D Plus dual target sequential sputtering system. Polypeptides were then imaged at 1000X and 3000X magnification.

Plate reader.

A Spark Multimodal Microplate Reader (TECAN) was used to determine the concentration of all drugs included in this study. Here, 100 µL of the analyte solution was dispensed in a well of a disposable 96-well plate (Greiner Bio-one UV-Star Microplate) and analyzed according to the following parameters. Absorbance spectra were acquired from 300–600 nm with a step size of 2 nm and a settle time of 50 ms. The λ_{max} was determined by identifying the wavelength at which the highest absorbance was recorded. These wavelengths are as follows: amitriptyline (AMI, 238 nm), bupropion (BUP, 252 nm), hydroxychloroquine (HCQ, 330 nm), and strychnine (STR, 254 nm). The absorbance of each drug following adsorption kinetics and capacity experiments was measured at these experimentally determined wavelengths and converted to concentration using calibration curves in accordance with Beer's Law (SI, Figures 19-26).

Nuclear magnetic resonance spectroscopy (^{1}H NMR).

A 500 MHz NMR (Bruker Avance™ 500) was used to acquire ^{1}H-NMR spectra of the monomers and polypeptides in DMSO-d6 and TFA-d. Data was analyzed using TopSpin TopSpin software (version 4.4.1).

Dynamic light scattering.

Dispersions of the polypeptides were prepared with a concentration of 50 μg/mL in SGF and SIF. The dispersions were then loaded into Malvern disposable folded capillary cells (DTS1070). Zeta potentials and particle sizes were measured using a Zetasizer Nano ZS (Malvern Instruments Ltd, Worcestershire, UK) with Zetasizer Software v7.12 (Malvern, Inc.). Three measurements were acquired using the optimal scanning parameters of the instrument (ranging from 10–100 scans per measurement).

METHODS

Synthesis of γ-benzyl-L-glutamate N-carboxyanhydride (Glu(OBzl)-NCA).

H-Glu(OBzl)-OH (2.00 g, 8.43 mmol, 1 eq) was added to an oven-dried flask and high vacuum was applied overnight to evaporate adsorbed moisture. The flask was refilled with dry N_2 and the amino acid was dispersed in dry THF to give a 0.1 M solution. Triphosgene (1.25 g, 4.21 mmol, 0.5 eq) was added in one shot under constant N2 flow. The reaction mixture was reacted at 50 ˚C for 3 h. The reaction mixture was then evaporated to dryness to give a pale yellow solid. The solid was redissolved in ethyl acetate, then consecutively washed with a mixture of 5% NaHCO3 and ice (2 X 50 mL), 5% HCl and ice (2 X 50 mL), and brine with no ice (1 X 50 mL). TLC was used to confirm the presence of Glu(OBzl)-NCA in the organic layer (Rf = 0.59, 100% ethyl acetate). The organic layer was then dried over $MgSO_4$ and evaporated to a concentrate. The concentrate was filtered through a silica plug into a flame-dried round bottom flask, and the plug was rinsed with ~100 mL of ethyl acetate. The solution was evaporated to a concentrate, put on ice, and hexanes was slowly added to precipitate the NCA. The precipitated NCA was vacuum filtered to give a white powder (1.85 g, 83% yield) which

was stored at 4 ˚C. The structure and purity of Glu(OBzl)-NCA were confirmed by ^{1}H-NMR (500 MHz) in DMSO-d6.

Synthesis of O-benzyl-L-tyrosine N-carboxyanhydride (Tyr(OBzl)-NCA).

H-Tyr(OBzl)-OH (2.40 g, 8.85 mmol, 1 eq) was added to an oven-dried flask and high vacuum was applied overnight to evaporate adsorbed moisture. The flask was refilled with dry N_2 and the amino acid was dispersed in dry THF to give a 0.1 M solution. Triphosgene (1.31 g, 4.42 mmol, 0.5 eq) was added in one shot under constant N2 flow. The reaction mixture was reacted at 50 ˚C for 5 h. The reaction mixture was then evaporated to dryness to give a green-white solid. The solid was redissolved in ethyl acetate, then consecutively washed with a mixture of 5% NaHCO3 and ice (2 X 50 mL), 5% HCl and ice (2 X 50 mL), and brine with no ice (1 X 50 mL). TLC was used to confirm the presence of Tyr(OBzl)-NCA in the organic layer (Rf = 0.44, 100% ethyl acetate). The organic layer was then dried over $MgSO_4$ and evaporated to a concentrate. The concentrate was filtered through a silica plug into a flame-dried round bottom flask, and the plug was rinsed with ~100 mL of ethyl acetate. The solution was evaporated to a concentrate, put on ice, and hexanes was slowly added to precipitate the NCA. The precipitated NCA was vacuum filtered to give a white powder (2.27 g, 86% yield) which was stored at 4 ˚C. The structure and purity and Tyr(OBzl)-NCA were confirmed by 1H-NMR (500 MHz) in DMSO-d6 (Figure S9).

Synthesis of E_{30} macroinitiator.

Glu(OBzl)-NCA (0.5690 g, 2.16 mmol, 30 equiv) was weighed into an oven-dried 50 mL round-bottom flask equipped with a magnetic stir bar and purged with dry nitrogen. The NCA was dissolved in 21.6 mL anhydrous N,N-dimethylformamide (DMF) to a final

concentration of 0.1 M under nitrogen. Separately, a solution of hexylamine initiator (29.4 mg/mL in anhydrous DMF) was prepared. 0.25 mL of the hexylamine solution (0.072 mmol, 1.0 equiv) was added to the NCA solution under a dry nitrogen atmosphere. The reaction was left to stir under inert atmosphere for 10 minutes. The flask was then placed under static vacuum for 5 minutes and returned to nitrogen. The reaction was allowed to proceed at room temperature for 36 hours, with the flask periodically uncapped every few hours to release CO_2 buildup and re-purged with dry nitrogen.

Synthesis of E30Y28 copolymer

Tyr(OBzl)-NCA (0.1135 g, 0.38 mmol, 30 equiv) was dissolved in dry DMF with stirring (0.05 M, 7.6 mL). The macroinitiator (3.86 mL, 0.013 mmol) was then added to the dissolved Tyr(OBzl)-NCA, with stirring. The reaction was left to stir under inert atmosphere for 10 minutes. The flask was then placed under static vacuum for 5 minutes and returned to nitrogen. The reaction was allowed to proceed at room temperature for 72 hours, with the flask periodically uncapped every few hours to release CO_2 buildup and re-purged with dry nitrogen. Upon completion, the reaction mixture was precipitated into cold diethyl ether (10-fold excess by volume), and the precipitated polymer was collected by centrifugation. The polymer was washed four times with cold diethyl ether (25 mL). The resulting poly[(γ-benzyl-L-glutamate)-*block*-(O-benzyl-L-tyrosine)] (pBzl-E30Y28) was dried under high vacuum to remove volatile organic compounds and solvent.

Synthesis of E30Y79 copolymer.

Tyr(OBzl)-NCA (0.3206 g, 1.08 mmol, 75 equiv) was dissolved in dry DMF with stirring (0.05 M, 22 mL). The macroinitiator (4.36 mL, 0.014 mmol) was then added to the

dissolved Tyr(OBzl)-NCA, with stirring. The reaction was left to stir under inert atmosphere for 10 minutes. The flask was then placed under static vacuum for 5 minutes and returned to nitrogen. The reaction was allowed to proceed at room temperature for 72 hours, with the flask periodically uncapped every few hours to release CO_2 buildup and re-purged with dry nitrogen. Upon completion, the reaction mixture was precipitated into cold diethyl ether (10-fold excess by volume), and the precipitated polymer was collected by centrifugation. The polymer was washed four times with cold diethyl ether (25 mL). The resulting poly[(γ-benzyl-L-glutamate)-*block*-(O-benzyl-L-tyrosine)] (pBzl-E30Y79) was dried under high vacuum to remove volatile organic compounds and solvent.

Synthesis of E30Y101 copolymer.

Tyr(OBzl)-NCA (0.2805 g, 0.94 mmol, 100 equiv) was dissolved in dry DMF with stirring (0.05 M, 19 mL). The macroinitiator (2.86 mL, 0.010 mmol) was then added to the dissolved Tyr(OBzl)-NCA, with stirring. The reaction was left to stir under inert atmosphere for 10 minutes. The flask was then placed under static vacuum for 5 minutes and returned to nitrogen. The reaction was allowed to proceed at room temperature for 72 hours, with the flask periodically uncapped every few hours to release CO_2 buildup and re-purged with dry nitrogen. Upon completion, the reaction mixture was precipitated into cold diethyl ether (10-fold excess by volume), and the precipitated polymer was collected by centrifugation. The polymer was washed four times with cold diethyl ether (25 mL). The resulting poly[(γ-benzyl-L-glutamate)-*block*-(O-benzyl-L-tyrosine)] (pBzl-E30Y101) was dried under high vacuum to remove volatile organic compounds and solvent.

Synthesis of E30Y129 copolymer.

Tyr(OBzl)-NCA (0.3506 g, 1.18 mmol, 125 equiv) was dissolved in dry DMF with stirring (0.05 M, 24 mL). The macroinitiator (2.86 mL, 0.010 mmol) was then added to the dissolved Tyr(OBzl)-NCA, with stirring. The reaction was left to stir under inert atmosphere for 10 minutes. The flask was then placed under static vacuum for 5 minutes and returned to nitrogen. The reaction was allowed to proceed at room temperature for 72 hours, with the flask periodically uncapped every few hours to release CO_2 buildup and re-purged with dry nitrogen. Upon completion, the reaction mixture was precipitated into cold diethyl ether (10-fold excess by volume), and the precipitated polymer was collected by centrifugation. The polymer was washed four times with cold diethyl ether (25 mL). The resulting poly[(γ-benzyl-L-glutamate)-*block*-(O-benzyl-L-tyrosine)] (pBzl-E30Y129) was dried under high vacuum to remove volatile organic compounds and solvent.

General deprotection of block copolymers

In an oven-dried round-bottom flask equipped with a magnetic stir bar, the protected polypeptide was added. The flask was purged with dry nitrogen gas to maintain an inert atmosphere. Trifluoroacetic acid was added to the flask to dissolve the polymer at a concentration of 100 mg/mL. The mixture was stirred until complete dissolution or until a uniform suspension was obtained. Separately, 48% aqueous hydrobromic acid (HBr) and glacial acetic acid (AcOH) were combined to achieve 33 wt. % solution of HBr in AcOH. This solution was added to the polypeptide in TFA under continuous stirring. The polypeptides were left to deprotect overnight. In the morning, polypeptides were precipitated in hexanes. Polypeptides were collected by centrifugation at 16,000 x g for

10 minutes. The pellet was then redissolved in dichloromethane, precipitated in hexanes, and centrifuged at 16,000 x g for 10 minutes twice. The polypeptides were then transferred to SnakeSkin™ dialysis tubing (molecular weight cutoff 3,500 Da). Dialysis was carried out against deionized water for 1 week, with water changes every 6 hours, to remove residual solvents, salts, and low-molecular-weight byproducts. After dialysis, the purified polypeptide was lyophilized to yield a white powder and stored at room temperature in a desiccator.

Adsorption studies.

Adsorption experiments (kinetics, capacity, and isotherm) were performed according to the following general procedure. Here, the polypeptide is termed “adsorbent;” drugs (amitriptyline (AMI), bupropion (BUP), hydroxychloroquine (HCQ), and strychnine (STR)) are termed “adsorbates;” and the buffer was either simulated gastric (pH 1.2) or simulated intestinal fluid (pH 6.8). Polypeptide materials were finely ground with a mortar and pestle prior to experimentation to ensure consistent particle sizes. Drug and polypeptide stock solutions were prepared fresh before each experiment to ensure accurate concentrations.

Adsorption kinetics experiments were performed using drug stock solutions at 0.5 mg/mL and polypeptide stock solutions at 1 mg/mL. Experimental samples (10:1 adsorbent-to-adsorbate mass ratio) were prepared using 135.7 µL of drug stock and 339.3 µL of polypeptide stock. Blanks were prepared using corresponding amounts of buffer in the absence of either drug or polypeptide stock. Adsorption capacity experiments were performed using drug stock solutions of 0.5 mg/mL and polypeptide stock solutions of 3 mg/mL. Experimental samples (13:1 adsorbent-to-adsorbate mass ratio) were

prepared using 271.4 µL of drug stock and 565.4 µL of polypeptide stock. Blanks were prepared using corresponding amounts of buffer in the absence of either drug or polypeptide stock. Adsorption isotherm experiments were performed using drug stock solutions of 0.5 mg/mL and polypeptide stock solutions of 4 mg/mL. Using these stock solutions, experimental samples were prepared by adding 100 µL of drug stock to different volumes of polypeptide stock, and adding the appropriate amount of buffer to ensure the same final volume for each sample. Blanks were prepared using corresponding amounts of buffer in the absence of either drug or polypeptide stock.

The fed-state adsorption experiments were performed according to the same protocol as the adsorption capacity experiments. However, these experiments were performed using a liquid baby food matrix calibrated to either pH 1.2 or pH 6.8 for the drug stock solution (Similac® 360 Total Care® RTF infant formula, 2 fl oz). This experimental design was chosen to more accurately reflect a fed gastrointestinal environment that drug is introduced into. Drugs were weighed into 20 mL scintillation vials and the pH-adjusted liquid baby food was added to prepare a drug stock solution of 0.5 mg/mL. The polypeptide stock solution was prepared according to standard procedures by weighing polypeptide into a 20 mL scintillation vial and suspending it in buffer at a concentration of 3 mg/mL. Experimental samples (13:1 adsorbent-to-adsorbate mass ratio) were prepared using 271.4 µL of drug stock and 565.4 µL of polypeptide stock. Matched control samples were prepared to account for matrix contributions to the UV–Vis signal, including drug-containing baby food without adsorbent and blanks containing adsorbent and baby food without drug. After background correction, absorbance values were converted to concentration using calibration curves generated in SGF or SIF. Under

these conditions, additional calibration curves prepared in the presence of baby food were not required. The samples were prepared using centrifugal filter units to remove any matrix components larger than 3 kDa. Further, the matrix and optical pathlength were dominated by the simulated biological media, and matrix contributions from the baby food were addressed using appropriate blanks. Adsorbates were readily soluble in buffer, based on concentration determined via Beer's Law using UV-Vis. Adsorbents were visually insoluble but could be homogeneously suspended by vortexing.

In a typical adsorption experiment, a known volume of polypeptide suspension was combined with a known volume of drug solution in a 1.8 mL Eppendorf tube. The drug concentration in the final mixture was calculated from known stock concentrations and volumes, while the initial free adsorbate concentration (C_0) was determined experimentally using control samples containing drug in the corresponding buffer without adsorbent. To begin the experiment, Eppendorf tubes were vortexed briefly to mix, then incubated at 37 °C (MyTemp Mini Digital Incubator, Benchmark Scientific) with rotational shaking (MiniMixer™, Benchmark Scientific). After a designated incubation period, the Eppendorf was centrifuged using centrifugal filter units (MWCO 3 kDa) at 16,000 × g for 15 min (Centrifuge 5418, Eppendorf) to filter soluble peptides and insoluble aggregates from the supernatant. Next, a 100 µL aliquot (containing the free adsorbate) was aspirated from the supernatant of the Eppendorf tube, and the aliquot was dispensed into a 96 well plate. Each supernatant was plated thrice (3 x 100 µL) with the standard deviation between triplicates reported using error bars in data charts. The absorbance of the supernatant was then analyzed using a plate reader, allowing determination of the concentration of free adsorbate in the supernatant (C_{eq}, µg/mL) using the linear

regression of calibration curves (SI, Figures 19-26). Using this and the experimentally determined initial concentration of adsorbate (C_o), Equations S1-3 were used to calculate the concentration of adsorbed adsorbent (C_{ads}, μg/mL), the percent of adsorbate adsorbed (% Ads), and the adsorption capacity (Q_e, mg adsorbent adsorbed per g adsorbent).

$$C_{ads} = C_o - C_{eq} \quad \textbf{Equation S1}$$

$$\% \, Ads \, = 100 \times \frac{C_{ads}}{C_o} \quad \textbf{Equation S2}$$

$$Q_e = \frac{C_{ads} \, x \, total \, volume}{adsorbent \, mass} \quad \textbf{Equation S3}$$

Cell culture

Lyophilized powders of polypeptide materials were sterilized in microcentrifuge tubes by exposure to 254 nm ultraviolet light for 10 minutes. For each material, approximately 2–3 mg was dissolved or dispersed in 1 mL of cell culture media via vortexing and sonication, followed by dilution to prepare 250 μg/mL stock solutions.

RAW 264.7 macrophages and NIH 3T3 fibroblasts were seeded into the interior wells of 96-well plates at a density of 2 x 10^4 cells/cm^2 and allowed to adhere for 2 hours. The culture medium was then aspirated and replaced with appropriate volumes of fresh media and material stock solutions to achieve a final volume of 200 μL per well and material concentrations of 250, 100, 10, and 1 μg/mL. All conditions were performed in triplicate. Cells were incubated for 48 hours prior to assessment of cellular viability.

Cell number, viability, and late-stage necrosis or apoptosis were evaluated using fluorescent reporters. Following incubation, media and materials were aspirated from the wells, and cells were washed twice with 100 µL of phosphate-buffered saline (PBS; catalog #10010023, ThermoFisher Scientific). Cells were then stained with a fluorescent solution consisting of PBS containing 20 mM Hoechst 33342 (catalog #62249, ThermoFisher Scientific), 2.5 mM Calcein AM (catalog #C3099, ThermoFisher Scientific), and 1.5 mM propidium iodide (catalog #J66584-AB, Alfa Aesar). After incubation for 10 minutes, the staining solution was removed and replaced with PBS.

Hoechst 33342 stains the DNA of all cell nuclei, enabling enumeration of total cell number. Calcein AM is converted to a fluorescent species by intracellular esterases following uptake, providing a measure of cell viability. Propidium iodide fluoresces upon binding DNA but is excluded from cells with intact membranes, thereby identifying dying cells that remain adherent. Fluorescence was quantified using a microplate reader with excitation/emission wavelengths of 350/450 nm (Hoechst), 485/525 nm (Calcein AM), and 530/620 nm (propidium iodide). Because plate-based fluorescence measurements can be unreliable in the presence of insoluble or fluorescence-modulating materials, direct fluorescence imaging was additionally performed using an EVOS® FL Auto Cell Imaging System equipped with a 20×, 0.30 numerical aperture objective. Images acquired in the DAPI channel (Hoechst) were analyzed using an in-house MATLAB cell-counting program, and the resulting cell counts were used to calculate percent viability.

CHARACTERIZATION

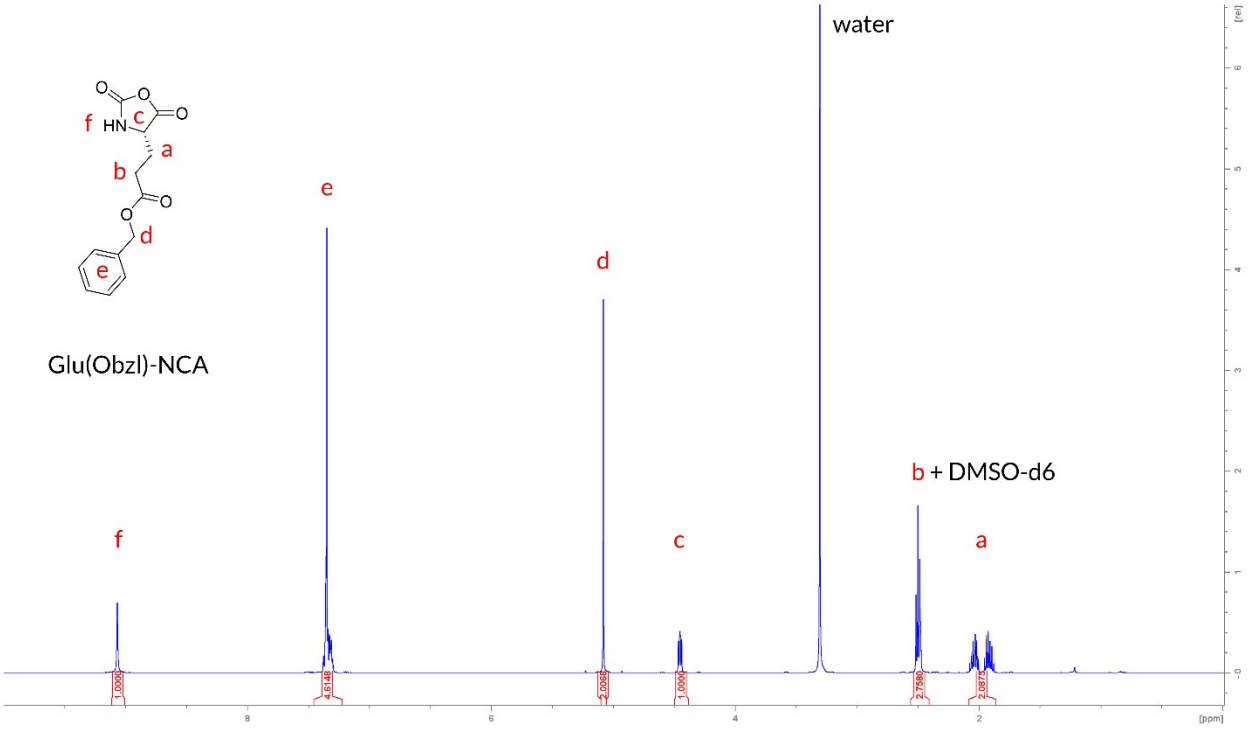

Figure S1. Annotated proton nuclear magnetic resonance (^{1}H NMR) spectrum of benzyl-protected glutamic acid N-carboxyanhydride (Glu(OBzl)-NCA) in deuterated dimethyl sulfoxide (DMSO-d_6). The spectrum is calibrated to the residual DMSO signal at ~2.50 ppm. The integrals are calibrated to the α-proton at ~4.45 ppm.

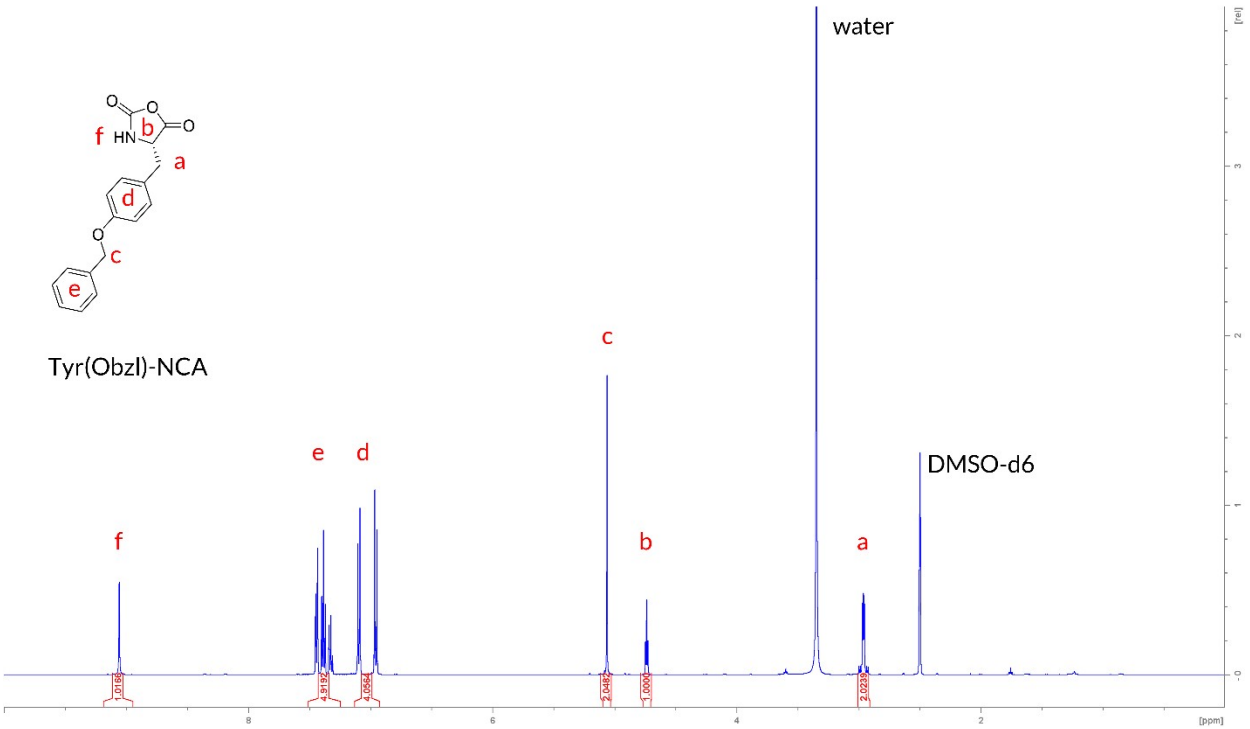

Figure S2. Annotated proton nuclear magnetic resonance (^{1}H NMR) spectrum of benzyl-protected tyrosine N-carboxyanhydride (Tyr(OBzl)-NCA) in deuterated dimethyl sulfoxide (DMSO-d_6). The spectrum is calibrated to the residual DMSO signal at ~2.50 ppm. The integrals are calibrated to the α-proton at ~4.70 ppm.

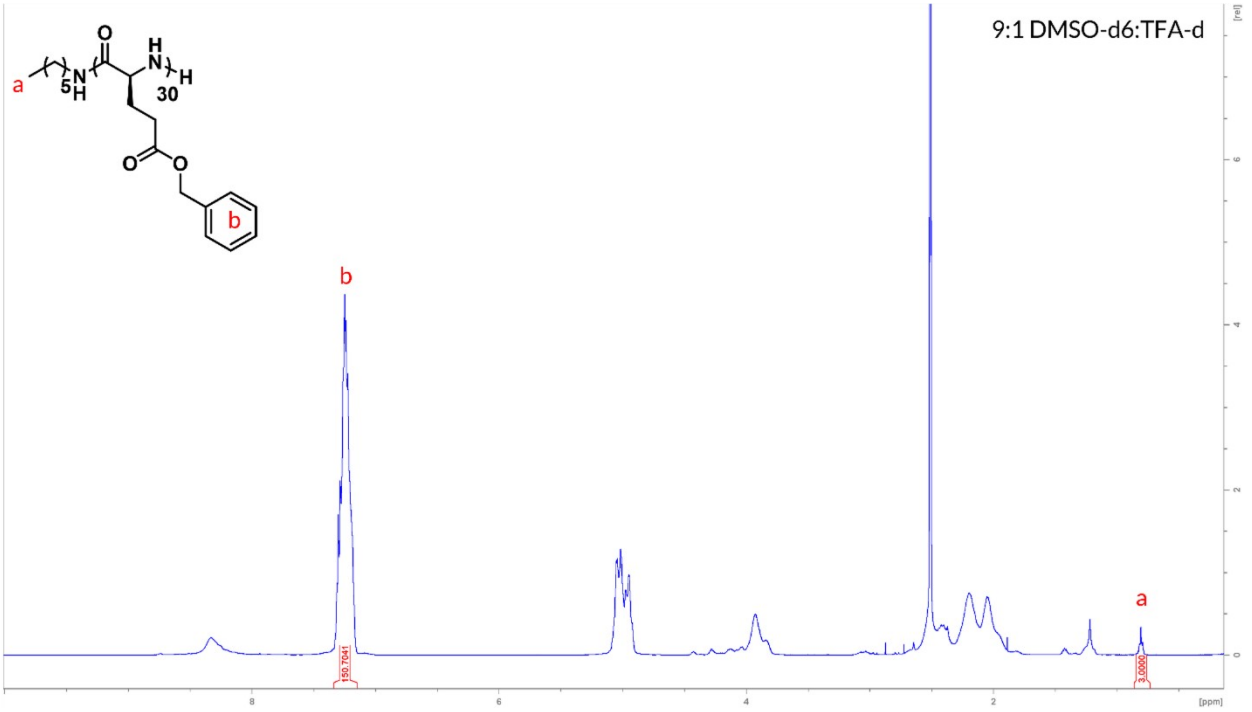

Figure S3. Proton nuclear magnetic resonance (^{1}H NMR) spectrum of the protected poly(glutamic acid) (pE30) macroinitiator in 9:1 deuterated dimethyl sulfoxide:deuterated trifluoroacetic acid (DMSO-d_6:TFA-d). The spectrum and integrals were calibrated to the hexylamine methyl end group at ~0.83 ppm (a). End group analysis referencing this signal was used to determine the degree of polymerization from the benzyl aromatic protons (b).

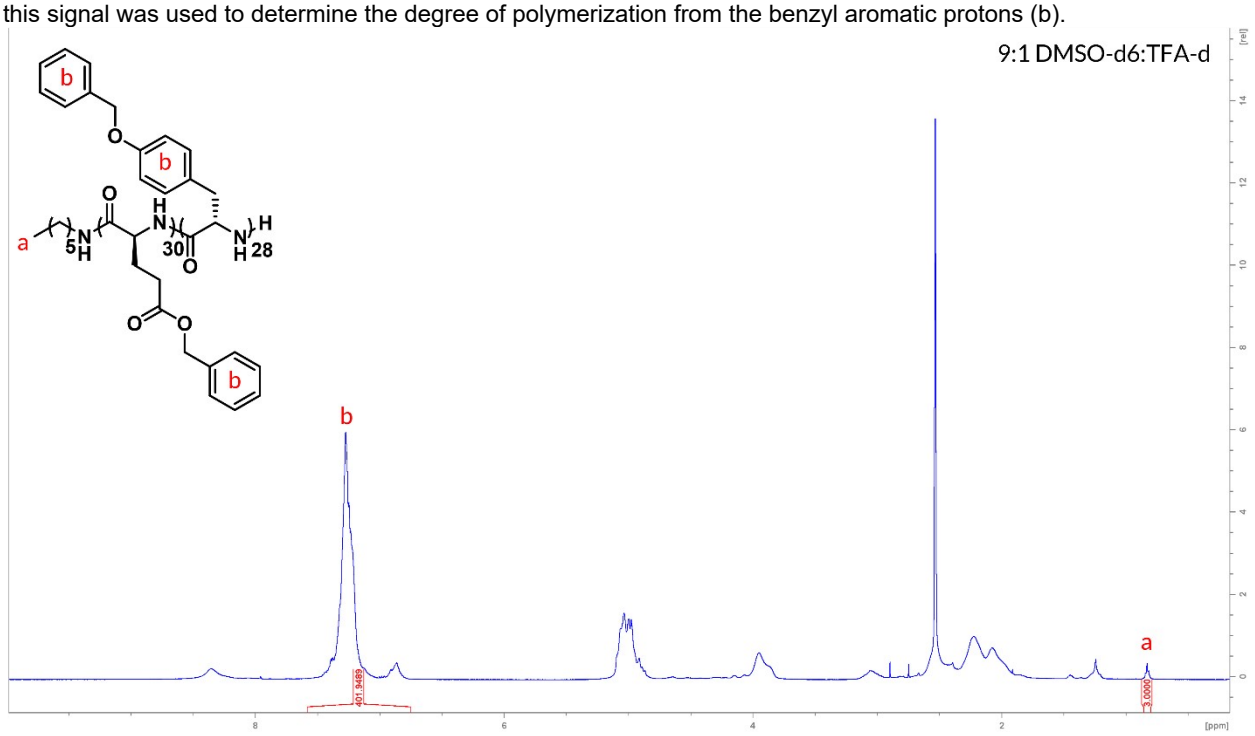

Figure S4. Proton nuclear magnetic resonance (^{1}H NMR) spectrum of protected E30Y28 in 9:1 deuterated dimethyl sulfoxide:deuterated trifluoroacetic acid (DMSO-d_6:TFA-d). The spectrum and integrals were calibrated to the hexylamine methyl end group at ~0.83 ppm (a). End group analysis referencing this signal was used to determine the degree of polymerization from the aromatic protons (b).

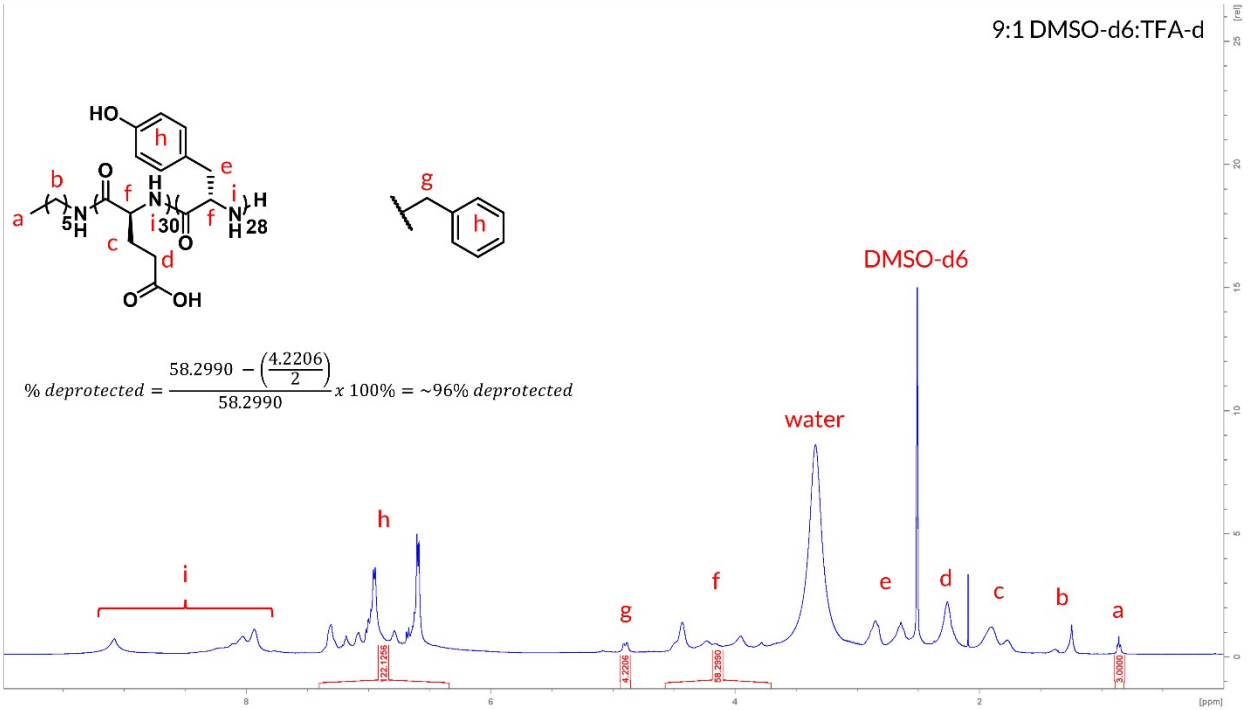

Figure S5. Annotated proton nuclear magnetic resonance (^{1}H NMR) spectrum of deprotected E30Y28 in 9:1 deuterated dimethyl sulfoxide:deuterated trifluoroacetic acid (DMSO-d_6:TFA-d). The spectrum was calibrated to the residual DMSO signal at ~2.50 ppm, and the integrals were calibrated to the hexylamine methyl end group at ~0.83 ppm (a). End group analysis referencing this signal was used to verify the degree of polymerization based on the remaining protecting group signal (g), backbone protons (f), and aromatic protons (h). The spectrum indicates that the polypeptide is ~96% deprotected.

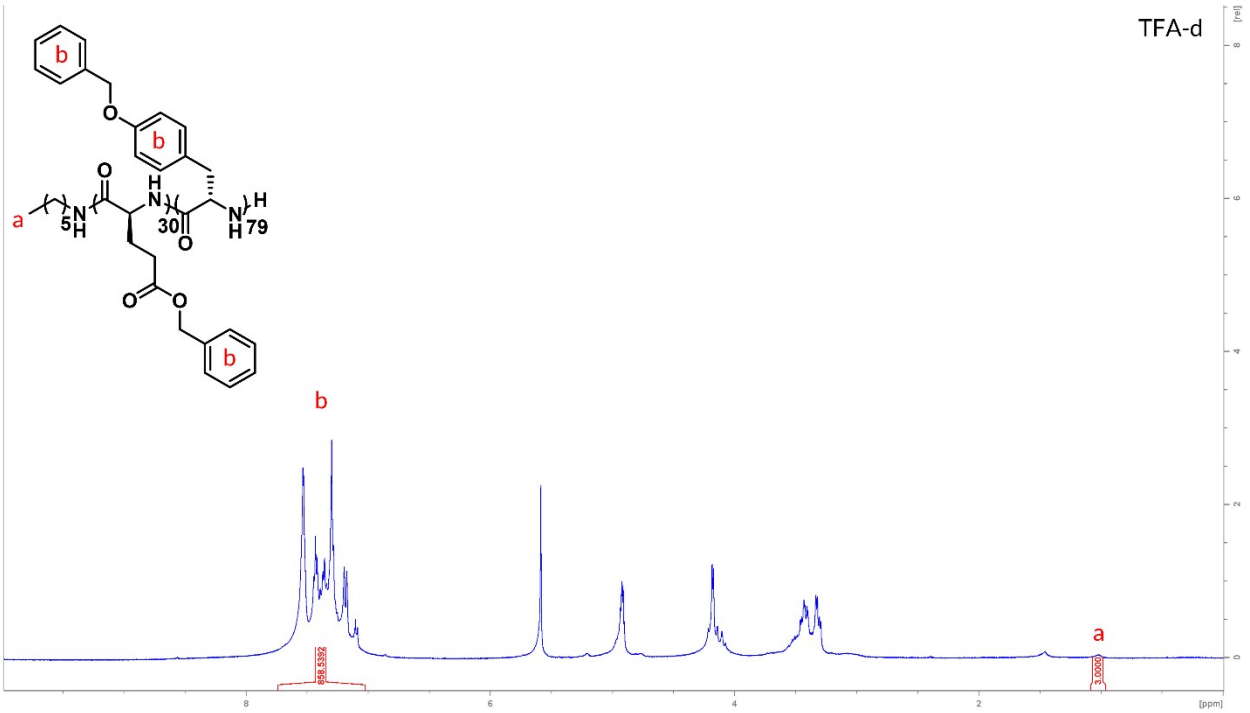

Figure S6. Proton nuclear magnetic resonance (^{1}H NMR) spectrum of protected E30Y79 in deuterated trifluoroacetic acid (TFA-d). The spectrum and integrals were calibrated to the hexylamine methyl end group at ~0.83 ppm (a). End group analysis referencing this signal was used to determine the degree of polymerization from the aromatic protons (b).

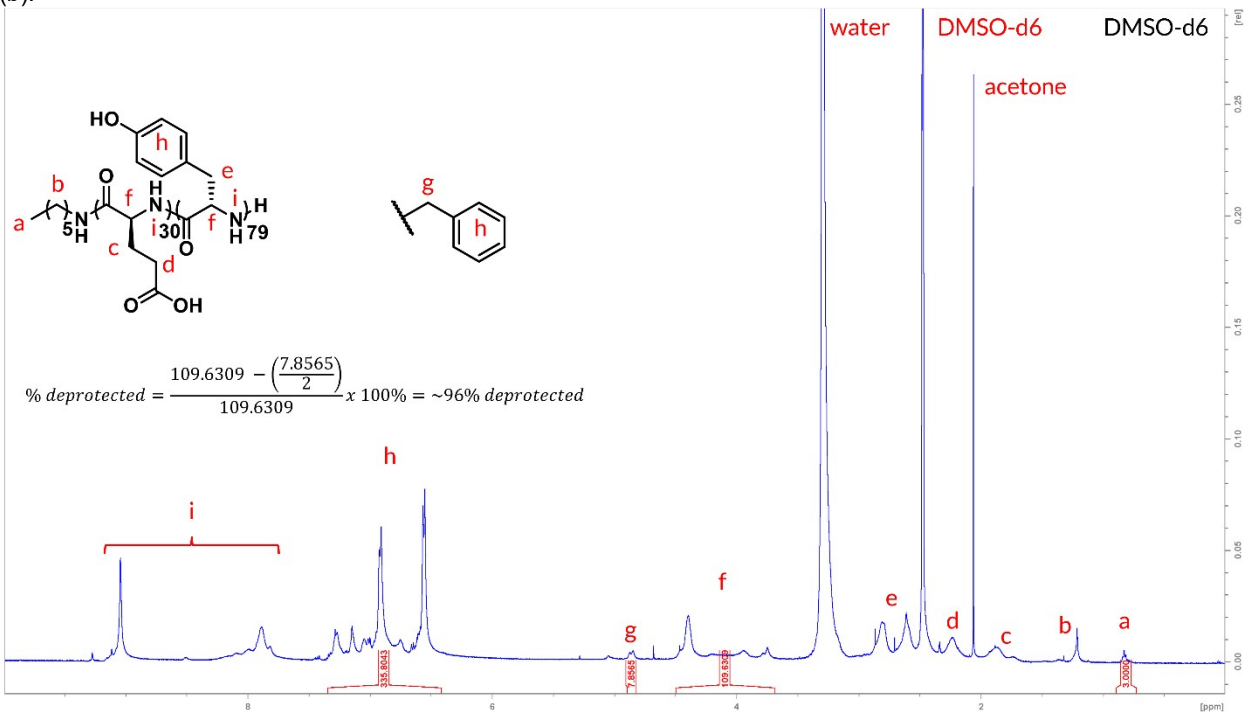

Figure S7. Annotated proton nuclear magnetic resonance (^{1}H NMR) spectrum of deprotected E30Y79 in deuterated dimethyl sulfoxide (DMSO-d_6). The spectrum was calibrated to the residual DMSO signal at ~2.50 ppm, and the integrals were calibrated to the hexylamine methyl end group at ~0.83 ppm (a). End group analysis referencing this signal was used to verify the degree of polymerization based on the remaining protecting group signal (g), backbone protons (f), and aromatic protons (h). The spectrum indicates that the polypeptide is ~96% deprotected.

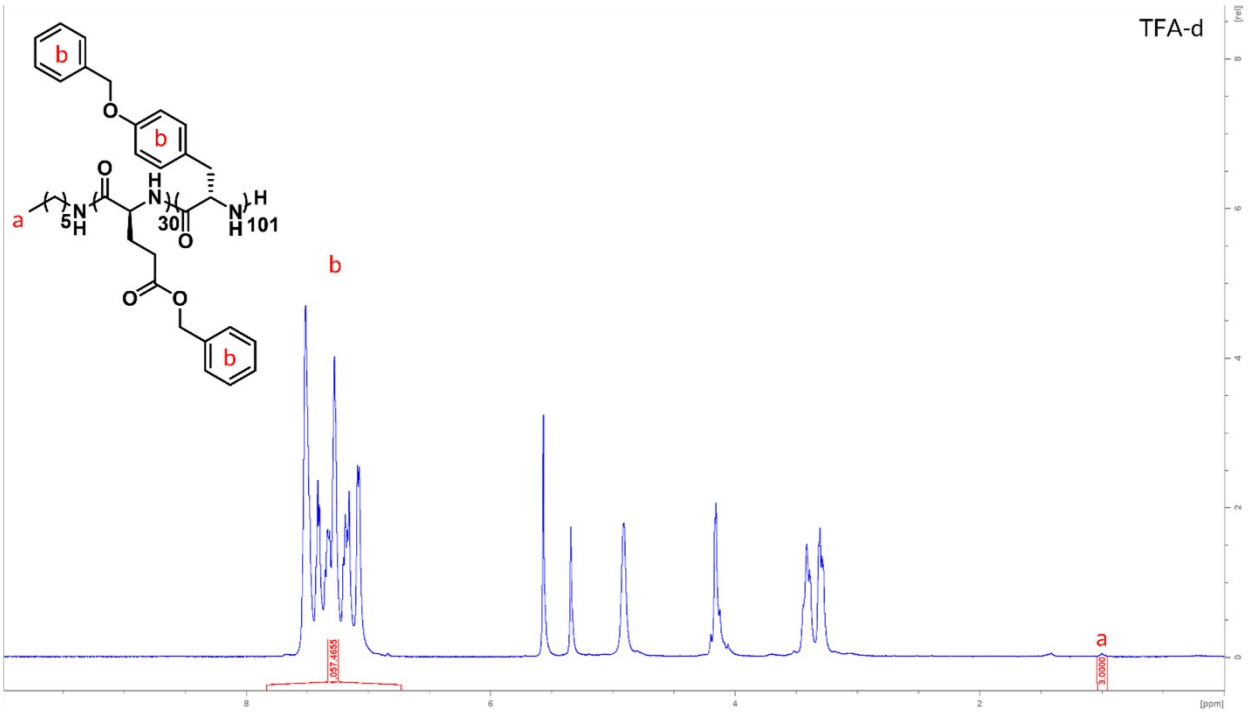

Figure S8. Proton nuclear magnetic resonance (^{1}H NMR) spectrum of protected E30Y101 in deuterated trifluoroacetic acid (TFA-d). The spectrum and integrals were calibrated to the hexylamine methyl end group at ~0.83 ppm (a). End group analysis referencing this signal was used to determine the degree of polymerization from the aromatic protons (b).

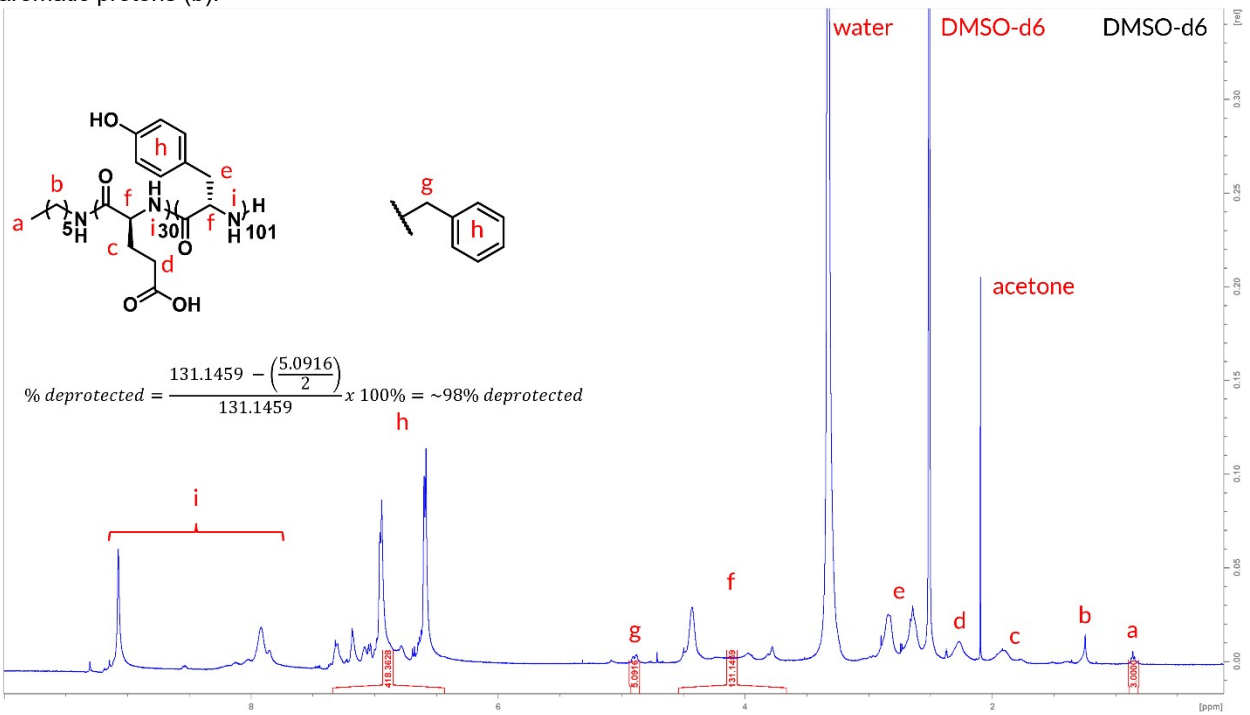

Figure S9. Annotated proton nuclear magnetic resonance (^{1}H NMR) spectrum of deprotected E30Y101 in deuterated dimethyl sulfoxide (DMSO-d_6). The spectrum was calibrated to the residual DMSO signal at ~2.50 ppm, and the integrals were calibrated to the hexylamine methyl end group at ~0.83 ppm (a). End group analysis referencing this signal was used to verify the degree of polymerization based on the remaining protecting group signal (g), backbone protons (f), and aromatic protons (h). The spectrum indicates that the polypeptide is ~98% deprotected.

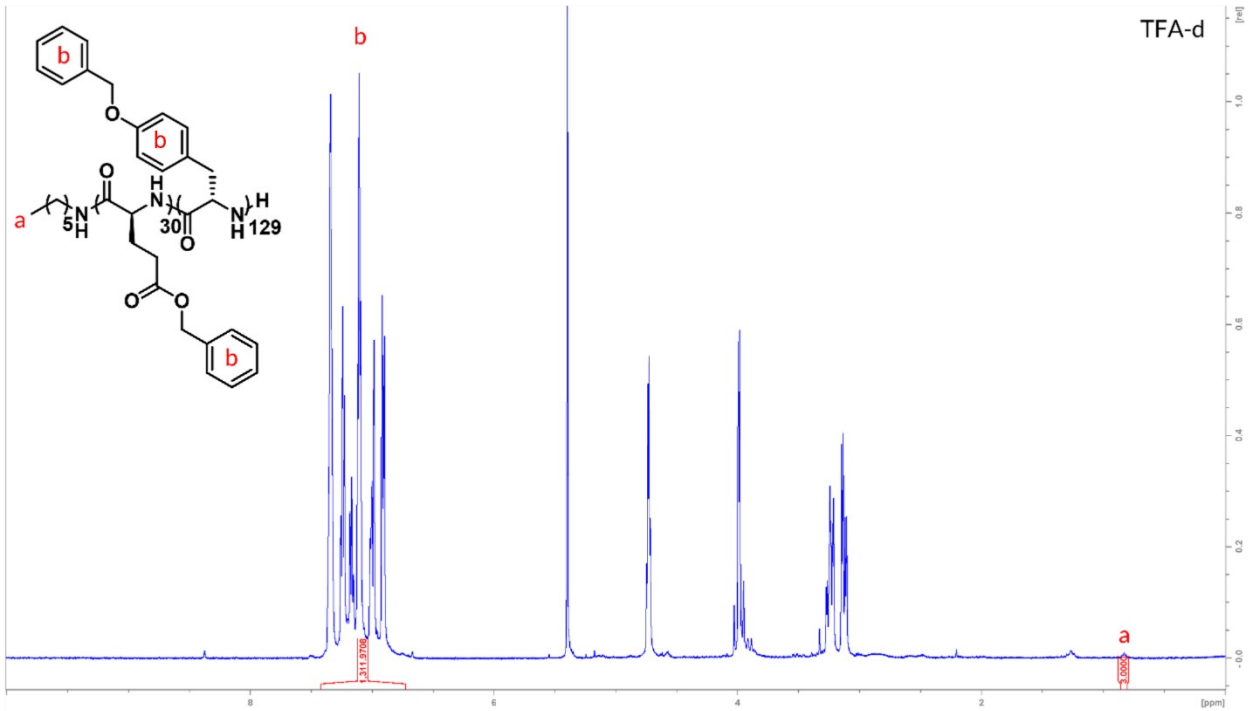

Figure S10. Proton nuclear magnetic resonance (^{1}H NMR) spectrum of protected E30Y129 in deuterated trifluoroacetic acid (TFA-d). The spectrum and integrals were calibrated to the hexylamine methyl end group at ~0.83 ppm (a). End group analysis referencing this signal was used to determine the degree of polymerization from the aromatic protons (b).

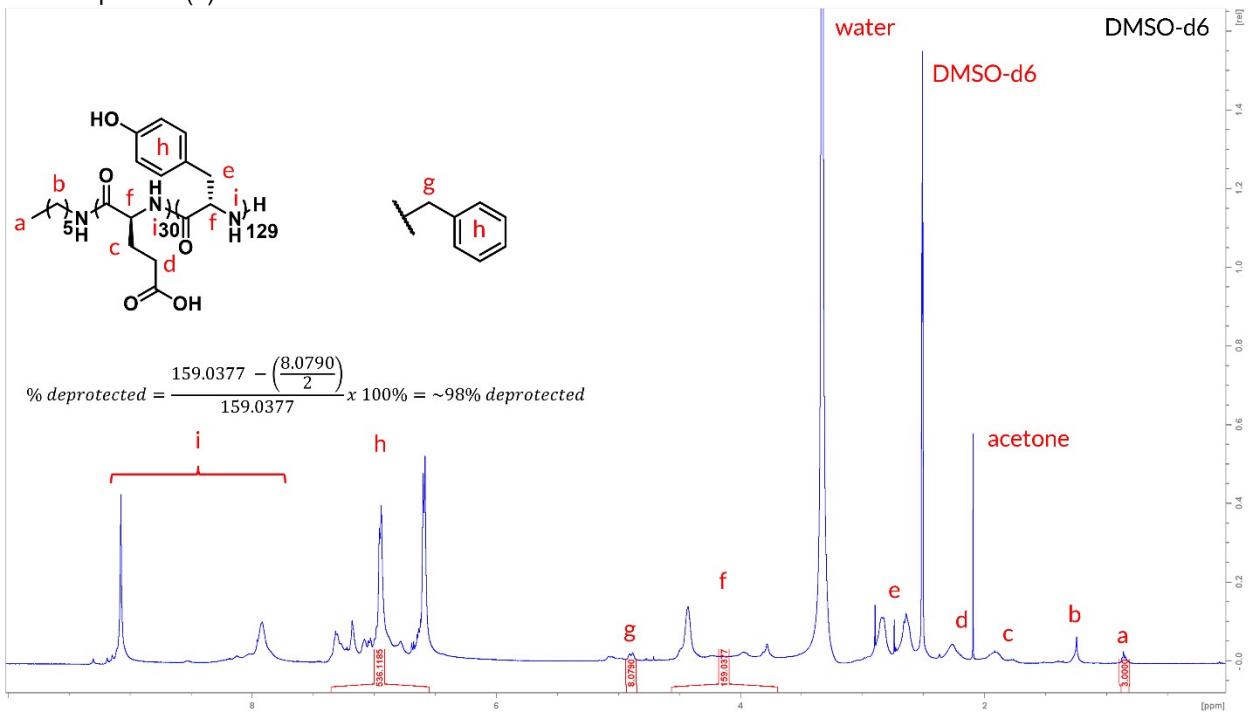

Figure S11. Annotated proton nuclear magnetic resonance (^{1}H NMR) spectrum of deprotected E30Y129 in deuterated dimethyl sulfoxide (DMSO-d_6). The spectrum was calibrated to the residual DMSO signal at ~2.50 ppm, and the integrals were calibrated to the hexylamine methyl end group at ~0.83 ppm (a). End group analysis referencing this signal was used to verify the degree of polymerization based on the remaining protecting group signal (g), backbone protons (f), and aromatic protons (h). The spectrum indicates that the polypeptide is ~98% deprotected.

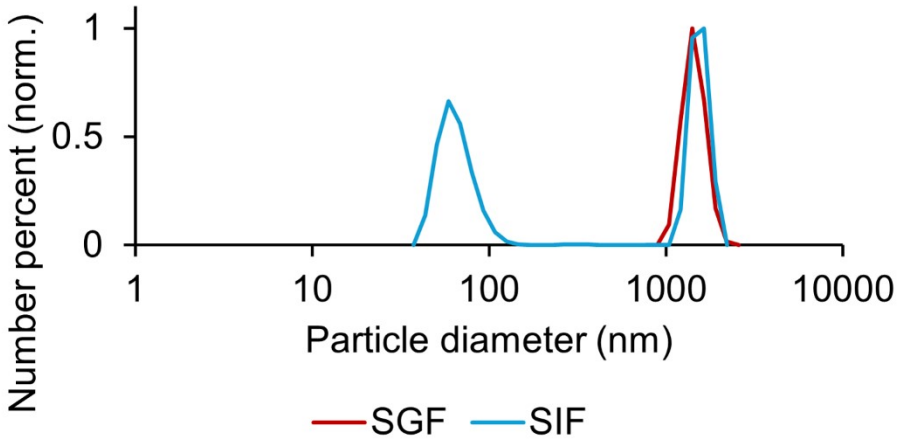

Figure S12. Particle size distribution of E30Y28 in simulated gastric fluid (SGF, pH 1.2) and simulated intestinal fluid(SIF, pH 6.8). Dynamic light scattering measurements were performed at 50 µg/mL in SGF and SIF. The SGF trace is dominated by a larger aggregate population above 1000 nm, while the SIF trace shows both a larger aggregate population above 1000 nm and a distinct lower diameter population below 100 nm. This lower diameter population supports the discussion of E30Y28 colloidal behavior in SIF and its exclusion from the primary SIF adsorption comparison. Particle size distributions are reported by number percent and are used as comparative descriptors under dilute measurement conditions.

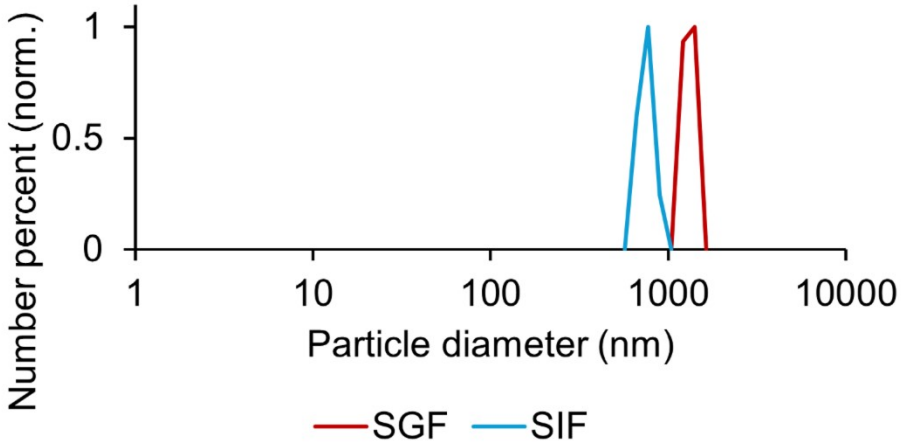

Figure S13. Particle size distribution of E30Y79 in simulated gastric fluid (SGF, pH 1.2) and simulated intestinal fluid (SIF, pH 6.8). Dynamic light scattering (DLS) measurements were performed at 50 µg/mL. Both traces show larger aggregate populations, with the SIF population shifted to lower particle diameter than the SGF population. Unlike E30Y28, E30Y79 does not show a distinct lower diameter population below 100 nm under these measurement conditions. Particle size distributions are shown as number percent distributions and are used as comparative descriptors under dilute measurement conditions.

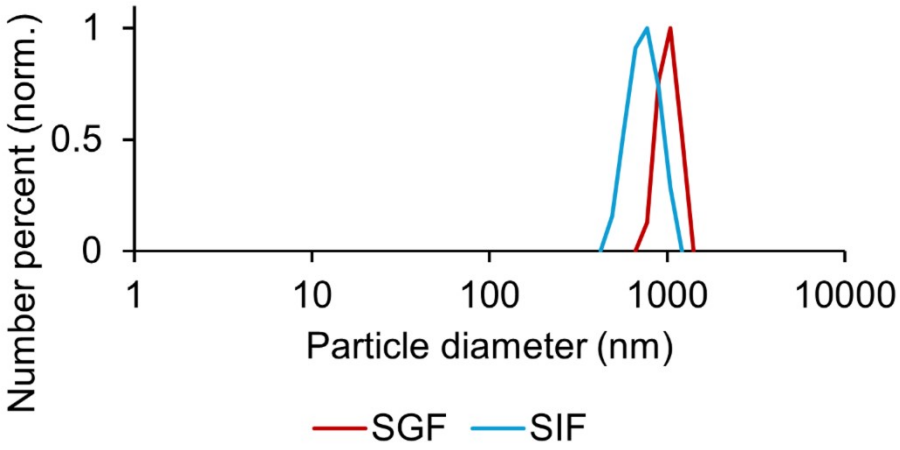

Figure S14. Particle size distribution of E30Y101 in simulated gastric fluid (SGF, pH 1.2) and simulated intestinal fluid (SIF, pH 6.8). Dynamic light scattering (DLS) measurements were performed at 50 µg/mL. Both traces show larger aggregate populations, with the SIF population shifted to lower particle diameter than the SGF population. Unlike E30Y28, E30Y101 does not show a distinct lower diameter population below 100 nm under these measurement conditions. Particle size distributions are shown as number percent distributions and are used as comparative descriptors under dilute measurement conditions.

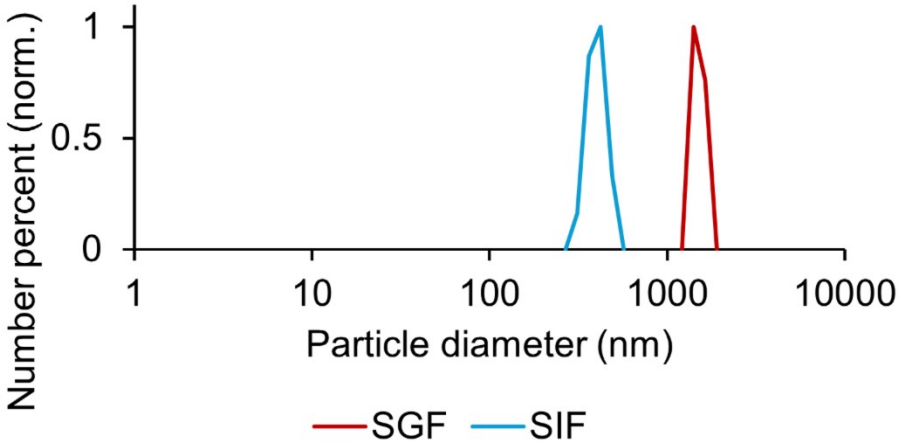

Figure S15. Particle size distribution of E30Y129 in simulated gastric fluid (SGF, pH 1.2) and simulated intestinal fluid (SIF, pH 6.8). Dynamic light scattering (DLS) measurements were performed at 50 µg/mL. Both traces show larger aggregate populations, with the SIF population shifted to lower particle diameter than the SGF population. Unlike E30Y28, E30Y129 does not show a distinct lower diameter population below 100 nm under these measurement conditions. Particle size distributions are shown as number percent distributions and are used as comparative descriptors under dilute measurement conditions.

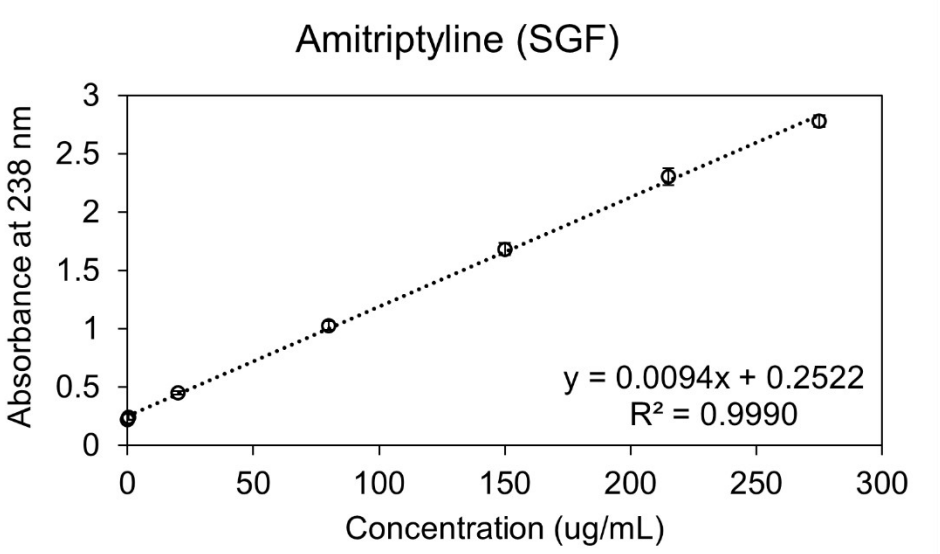

Figure S16. Calibration curve for amitriptyline (AMI) in simulated gastric fluid (SGF, pH 1.2). Absorbance was measured by ultraviolet-visible (UV-Vis) spectroscopy at 238 nm and plotted as a function of AMI concentration. The linear fit was used to convert absorbance values to free AMI concentrations in adsorption experiments performed in SGF.

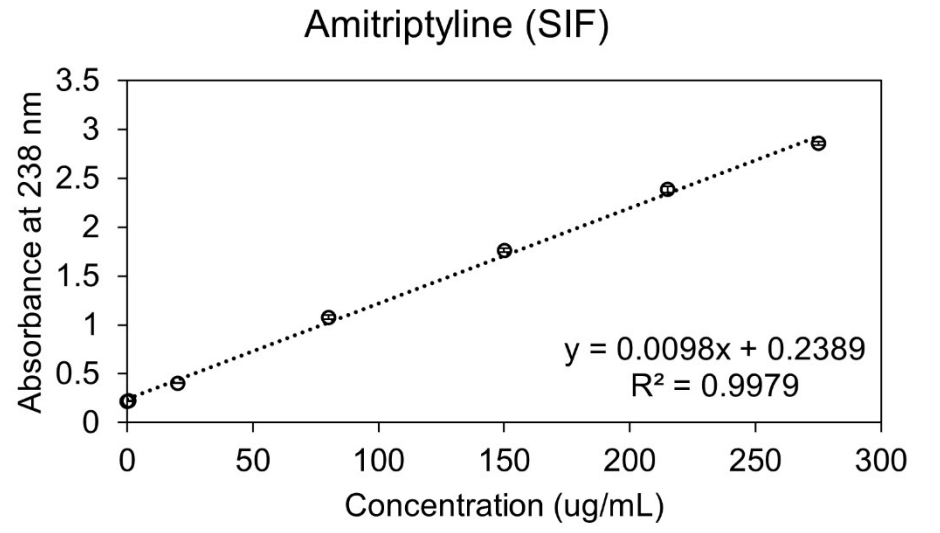

Figure S17. Calibration curve for amitriptyline (AMI) in simulated intestinal fluid (SIF, pH 6.8). Absorbance was measured by ultraviolet-visible (UV-Vis) spectroscopy at 238 nm and plotted as a function of AMI concentration. The linear fit was used to convert absorbance values to free AMI concentrations in adsorption experiments performed in SIF.

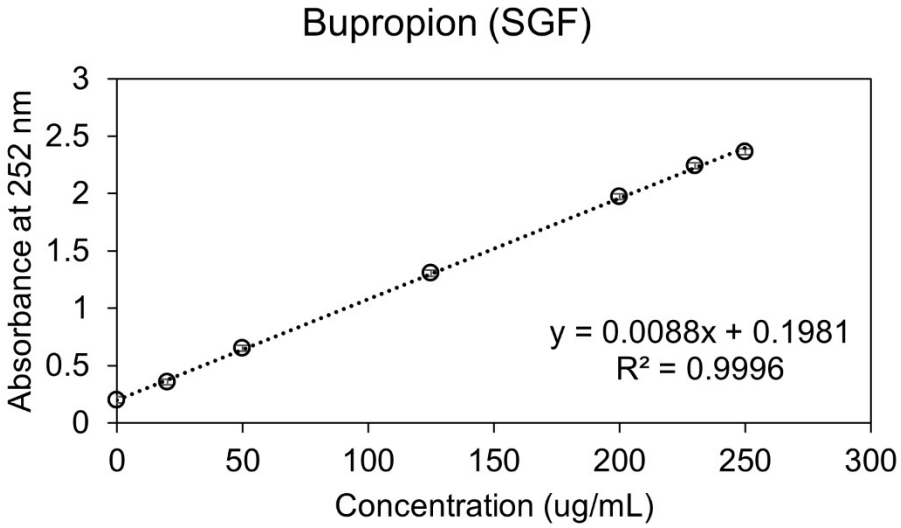

Figure S18. Calibration curve for bupropion (BUP) in simulated gastric fluid (SGF, pH 1.2). Absorbance was measured by ultraviolet-visible (UV-Vis) spectroscopy at 252 nm and plotted as a function of BUP concentration. The linear fit was used to convert absorbance values to free BUP concentrations in adsorption experiments performed in SGF.

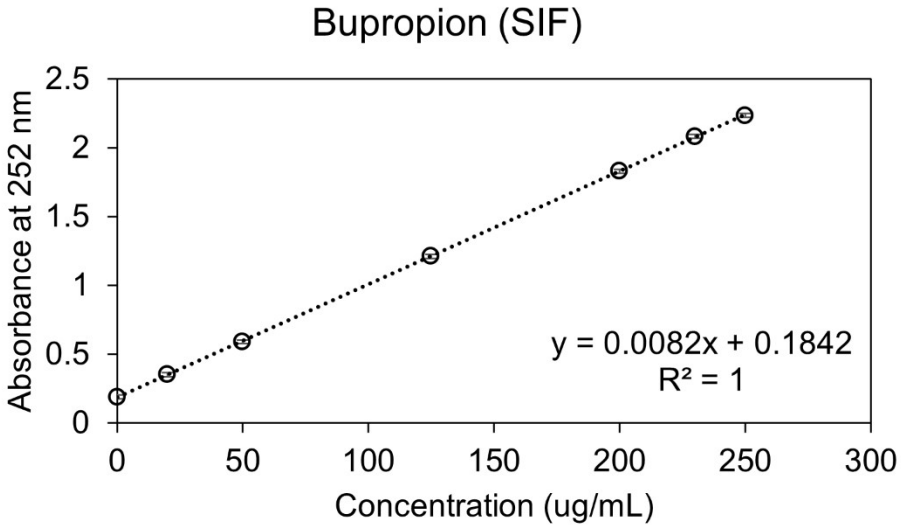

Figure S19. Calibration curve for bupropion (BUP) in simulated intestinal fluid (SIF, pH 6.8). Absorbance was measured by ultraviolet-visible (UV-Vis) spectroscopy at 252 nm and plotted as a function of BUP concentration. The linear fit was used to convert absorbance values to free BUP concentrations in adsorption experiments performed in SIF.

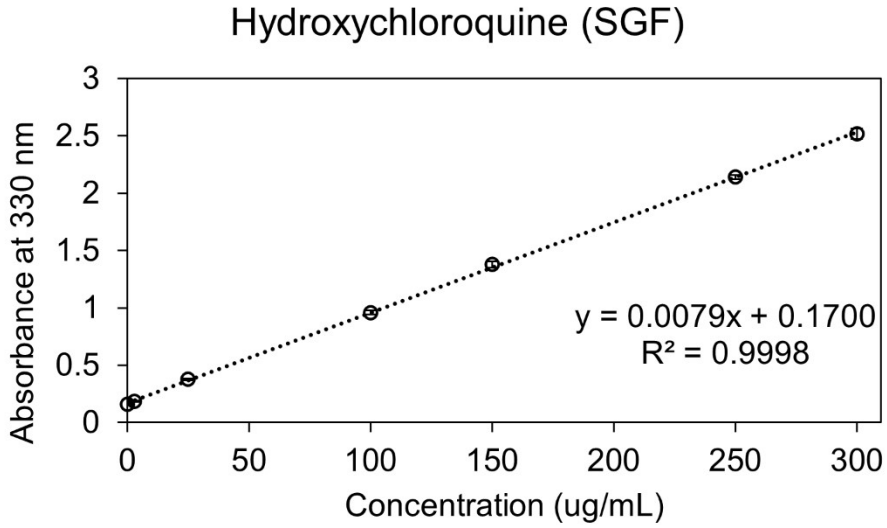

Figure S20. Calibration curve for hydroxychloroquine (HCQ) in simulated gastric fluid (SGF, pH 1.2). Absorbance was measured by ultraviolet-visible (UV-Vis) spectroscopy at 330 nm and plotted as a function of HCQ concentration. The linear fit was used to convert absorbance values to free HCQ concentrations in adsorption experiments performed in SGF.

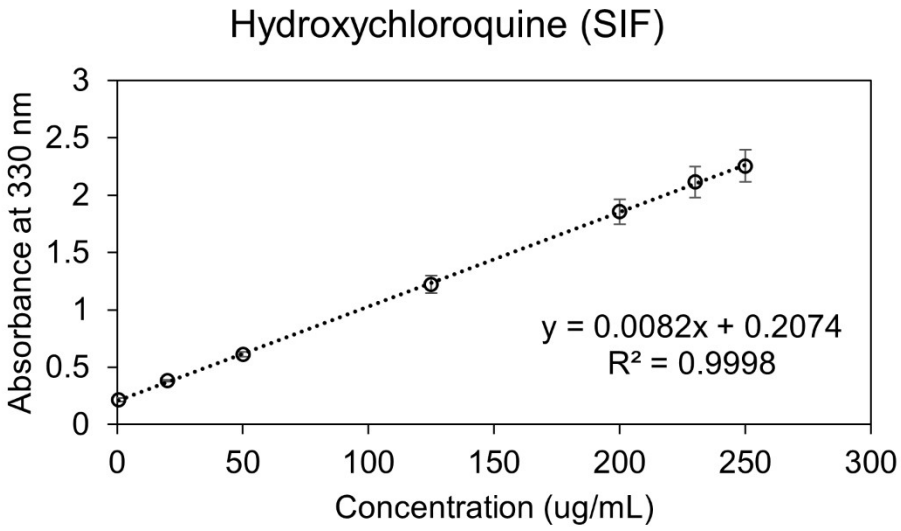

Figure S21. Calibration curve for hydroxychloroquine (HCQ) in simulated intestinal fluid (SIF, pH 6.8). Absorbance was measured by ultraviolet-visible (UV-Vis) spectroscopy at 330 nm and plotted as a function of HCQ concentration. The linear fit was used to convert absorbance values to free HCQ concentrations in adsorption experiments performed in SIF.

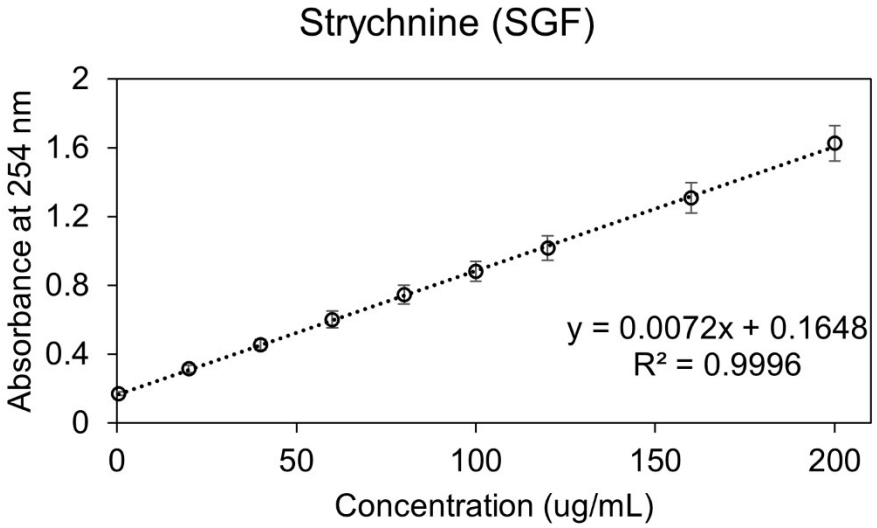

Figure S22. Calibration curve for strychnine (STR) in simulated gastric fluid (SGF, pH 1.2). Absorbance was measured by ultraviolet-visible (UV-Vis) spectroscopy at 254 nm and plotted as a function of STR concentration. The linear fit was used to convert absorbance values to free STR concentrations in adsorption experiments performed in SGF.

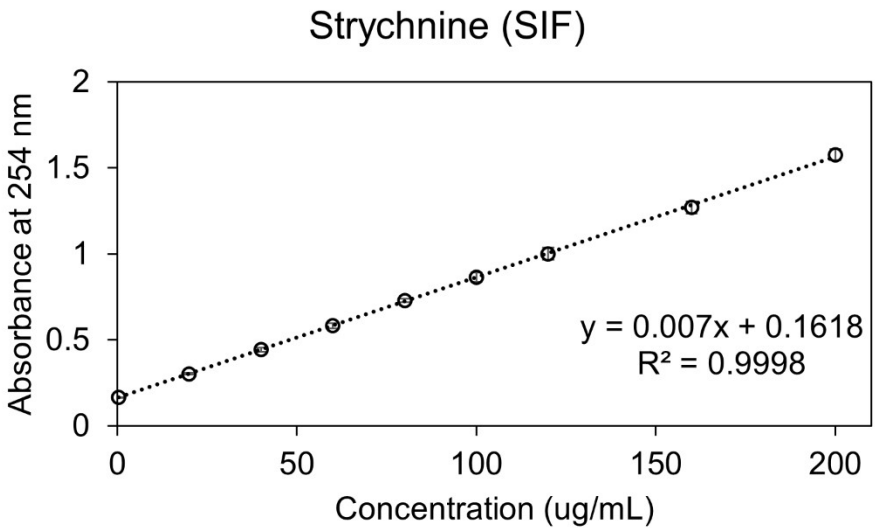

Figure S23. Calibration curve for strychnine (STR) in simulated intestinal fluid (SIF, pH 6.8). Absorbance was measured by ultraviolet-visible (UV-Vis) spectroscopy at 254 nm and plotted as a function of STR concentration. The linear fit was used to convert absorbance values to free STR concentrations in adsorption experiments performed in SIF.

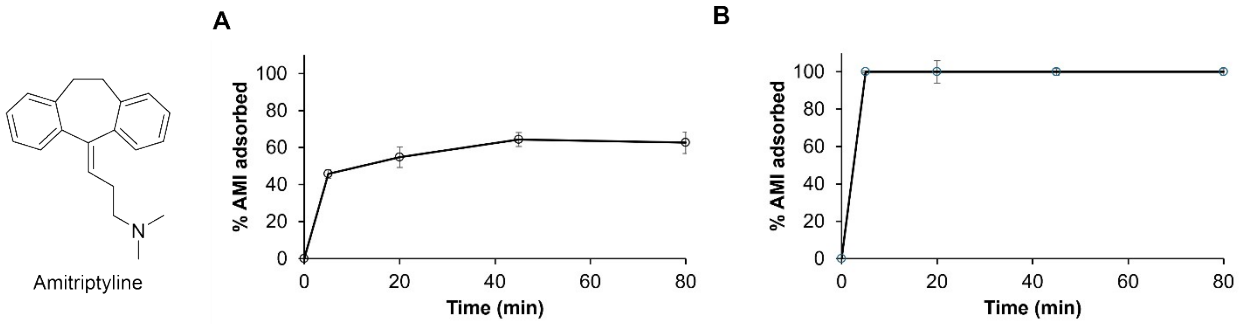

Figure S24. Adsorption kinetics for amitriptyline (AMI) adsorption to E30Y129 in A) simulated gastric fluid (SGF, pH 1.2) and B) simulated intestinal fluid (SIF, pH 6.8). Adsorption experiments were performed at 37 °C using a 10:1 adsorbent to adsorbate mass ratio. AMI adsorption occurred more rapidly in SIF than in SGF, consistent with the pH-dependent adsorption behavior discussed in the main text. Data are shown as mean ± standard deviation from triplicate measurements.

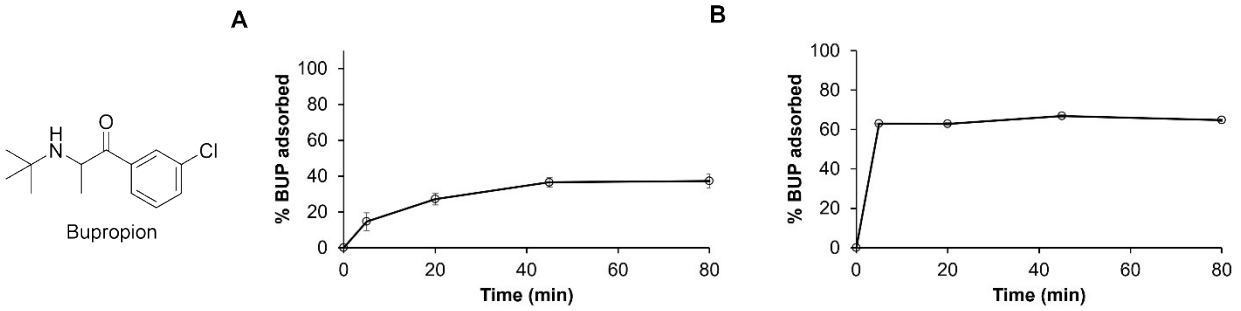

Figure S25. Adsorption kinetics for bupropion (BUP) adsorption to E30Y129 in A) simulated gastric fluid (SGF, pH 1.2) and B) simulated intestinal fluid (SIF, pH 6.8). Adsorption experiments were performed at 37 °C using a 10:1 adsorbent to adsorbate mass ratio. BUP adsorption occurred more rapidly in SIF than in SGF, consistent with the pH-dependent adsorption behavior discussed in the main text. Data are shown as mean ± standard deviation from triplicate measurements.

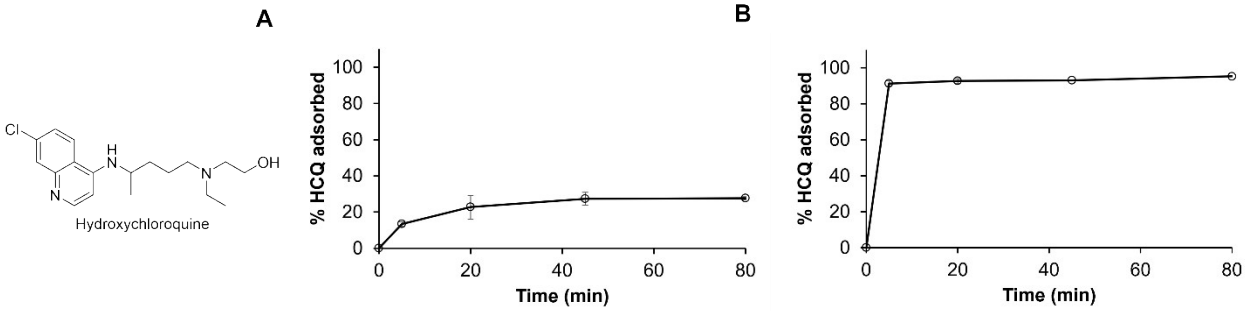

Figure S26. Adsorption kinetics for hydroxychloroquine (HCQ) adsorption to E30Y129 in A) simulated gastric fluid (SGF, pH 1.2) and B) simulated intestinal fluid (SIF, pH 6.8). Adsorption experiments were performed at 37 °C using a 10:1 adsorbent to adsorbate mass ratio. HCQ adsorption occurred more rapidly in SIF than in SGF, consistent with the pH-dependent adsorption behavior discussed in the main text. Data are shown as mean ± standard deviation from triplicate measurements.

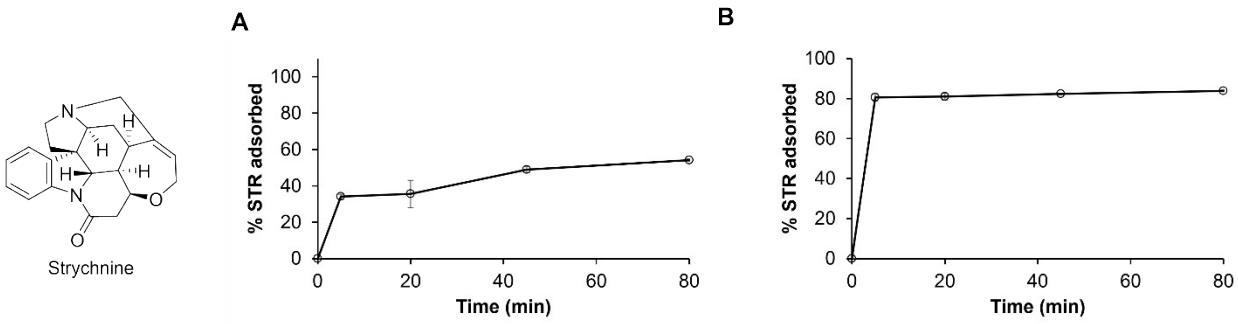

Figure S27. Adsorption kinetics for strychnine (STR) adsorption to E30Y129 in A) simulated gastric fluid (SGF, pH 1.2) and B) simulated intestinal fluid (SIF, pH 6.8). Adsorption experiments were performed at 37 °C using a 10:1 adsorbent to adsorbate mass ratio. STR adsorption occurred more rapidly in SIF than in SGF, consistent with the pH-dependent adsorption behavior discussed in the main text. Data are shown as mean ± standard deviation from triplicate measurements.

Figure S28. Representative photograph of E30Y28 dispersed in deionized water adjusted to pH 8. The suspension appears turbid but visually homo tographed conditions. This appearance is consistent with c sion of its distinct solution behavior.

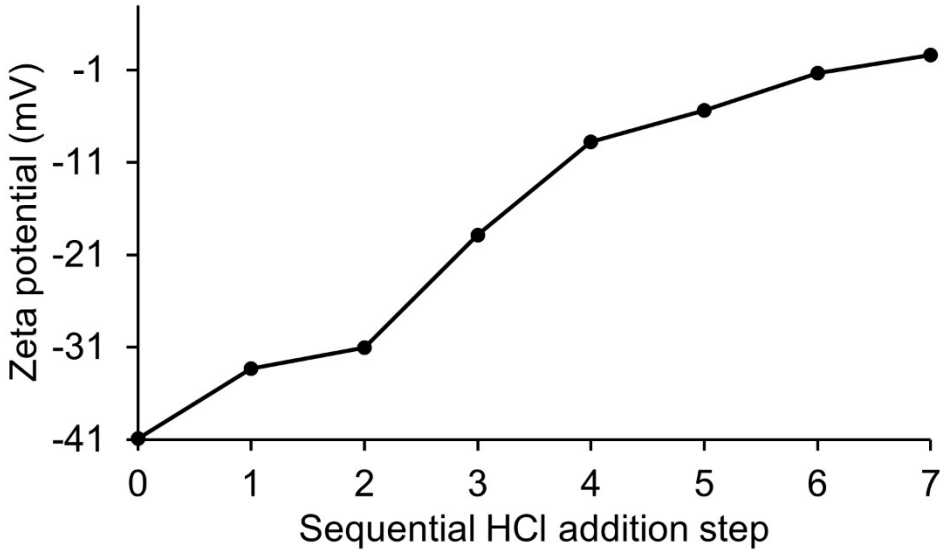

Figure S29. Zeta potential of E30Y28 during sequential acidification from pH 8. E30Y28 was dispersed at 1 mg/mL in deionized water adjusted to pH 8, followed by sequential additions of dilute hydrochloric acid (HCl). Step 0 shows the initial zeta potential before HCl addition, and subsequent steps correspond to successive HCl additions. Data are plotted by acid addition step because pH was not measured after each addition. The surface charge becomes progressively less negative with acid addition, consistent with protonation of negatively charged glutamic acid side chains.

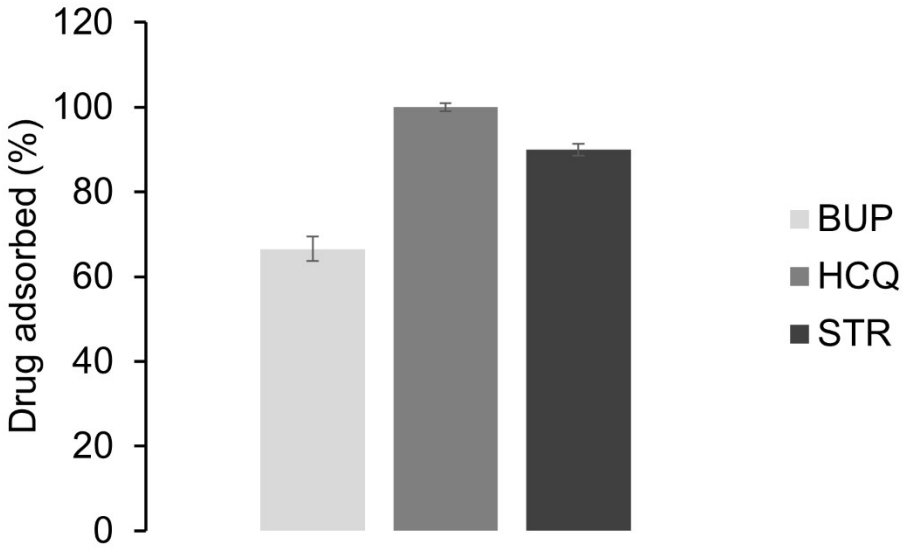

Figure S30. Apparent adsorption of bupropion (BUP), hydroxychloroquine (HCQ), and strychnine (STR) by E30Y28 in simulated intestinal fluid (SIF, pH 6.8). Adsorption was determined by ultraviolet visible (UV-Vis) analysis of the post-adsorption filtrate following centrifugal filtration. These data are provided for transparency but were not included in the Figure 4 comparison with E30Y79, E30Y101, and E30Y129 because E30Y28 exhibited a distinct particle population below 100 nm (Supplementary Figure S12, blue, <100 nm) and filter passing behavior that complicated direct comparison with the longer tyrosine block materials. In contrast, E30Y79, E30Y101, and E30Y129 showed larger aggregate populations under the same dilute particle size measurement conditions. Bars represent mean ± standard deviation from triplicate measurements.

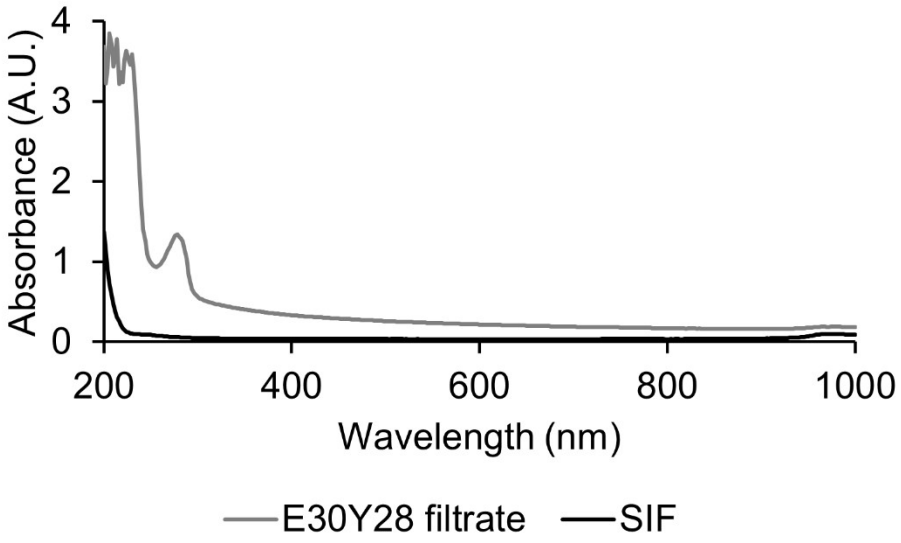

Figure S31. Absorbance of filtrate from E30Y28 suspended in simulated intestinal fluid (SIF, pH 6.8) compared to SIF alone after centrifugal filtration using 3 kDa molecular weight cutoff (MWCO) filters. The increased absorbance of the E30Y28 filtrate indicates that species from E30Y28 remained in the filtrate after centrifugal filtration. This filter passing behavior is consistent with the lower diameter population below 100 nm observed for E30Y28 in SIF by dynamic light scattering (Figure S12, blue, <100 nm).

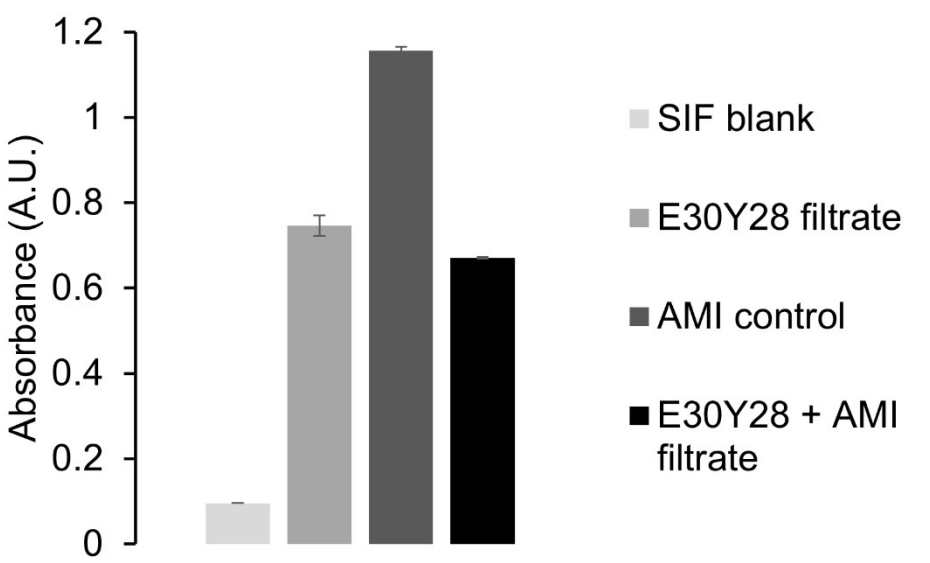

Figure S32. Absorbance at 238 nm for blank media, the amitriptyline (AMI) starting concentration, E30Y28 filtrate, and the post adsorption filtrate following incubation of AMI with E30Y28 in simulated intestinal fluid (SIF, pH 6.8). E30Y28 was suspended in SIF and centrifuged using a 3 kDa molecular weight cutoff (MWCO) filter in the absence or presence of AMI. The E30Y28-only filtrate showed measurable absorbance at 238 nm, indicating that E30Y28 derived species remained in the filtrate after centrifugal filtration. Because the E30Y28 only filtrate absorbance was greater than the absorbance of the E30Y28 + AMI post adsorption filtrate, ultraviolet visible (UV-Vis) quantification of free AMI was not reliable using blank correction. These data support the decision not to report apparent AMI adsorption to E30Y28 in SIF (Supplementary Figure S30).

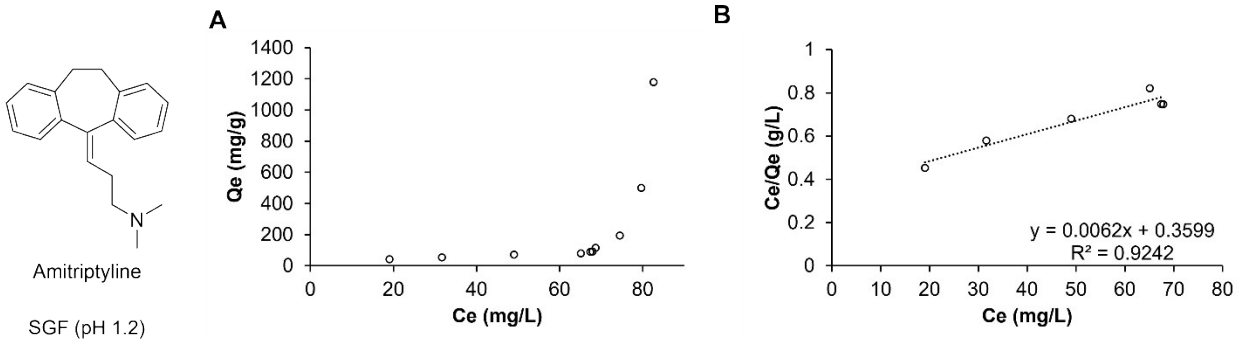

Figure S33. Adsorption isotherm analysis for amitriptyline (AMI) adsorption to E30Y129 in simulated gastric fluid (SGF, pH 1.2). A) shows the nonlinear adsorption isotherm plotted as equilibrium adsorption capacity (Q_e) versus equilibrium concentration (C_e). B) shows the linearized Langmuir fit applied to the low C_e region to derive apparent maximum adsorption capacity (Q_{max}) and apparent binding affinity (K_L). The fitted parameters are used as comparative descriptors for the low concentration adsorption regime and do not capture non ideal adsorption behavior observed at higher C_e values.

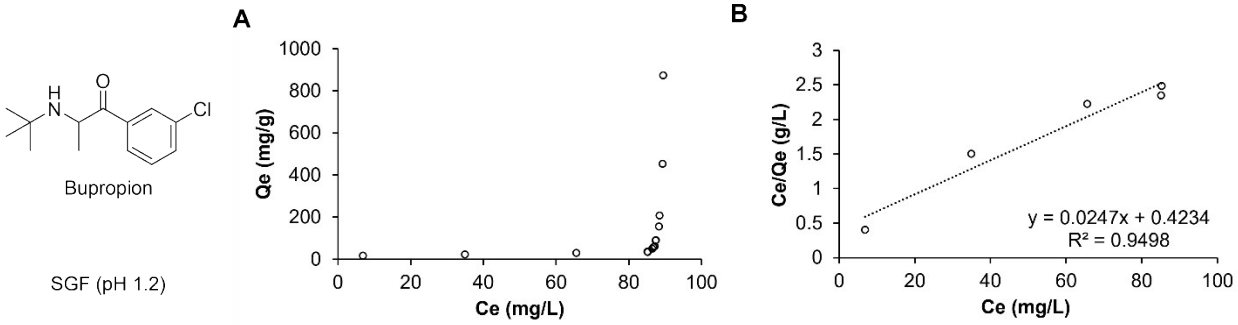

Figure S34. Adsorption isotherm analysis for bupropion (BUP) adsorption to E30Y129 in simulated gastric fluid (SGF, pH 1.2). A) shows the nonlinear adsorption isotherm plotted as equilibrium adsorption capacity (Q_e) versus equilibrium concentration (C_e). B) shows the linearized Langmuir fit applied to the low C_e region to derive apparent maximum adsorption capacity (Q_{max}) and apparent binding affinity (K_L). The fitted parameters are used as comparative descriptors for the low concentration adsorption regime and do not capture non ideal adsorption behavior observed at higher C_e values.

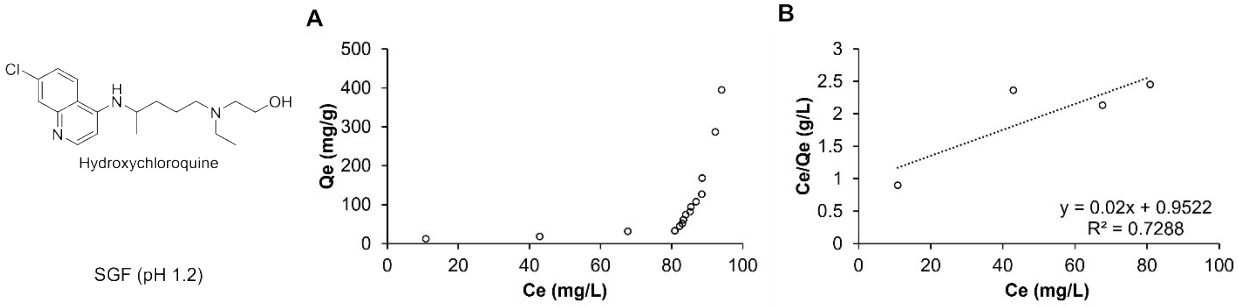

Figure S35. Adsorption isotherm analysis for hydroxychloroquine (HCQ) adsorption to E30Y129 in simulated gastric fluid (SGF, pH 1.2). A) shows the nonlinear adsorption isotherm plotted as equilibrium adsorption capacity (Q_e) versus equilibrium concentration (C_e). B) shows the linearized Langmuir fit applied to the low C_e region to derive apparent maximum adsorption capacity (Q_{max}) and apparent binding affinity (K_L). The fitted parameters are used as comparative descriptors for the low concentration adsorption regime and do not capture non ideal adsorption behavior observed at higher C_e values.

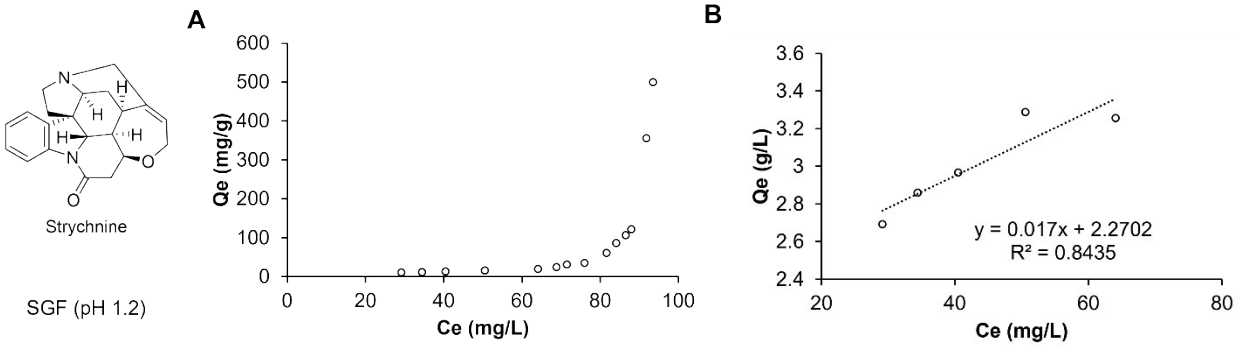

Figure S36. Adsorption isotherm analysis for strychnine (STR) adsorption to E30Y129 in simulated gastric fluid (SGF, pH 1.2). A) shows the nonlinear adsorption isotherm plotted as equilibrium adsorption capacity (Q_e) versus equilibrium concentration (C_e). B) shows the linearized Langmuir fit applied to the low C_e region to derive apparent maximum adsorption capacity (Q_{max}) and apparent binding affinity (K_L). The fitted parameters are used as comparative descriptors for the low concentration adsorption regime and do not capture non ideal adsorption behavior observed at higher C_e values.

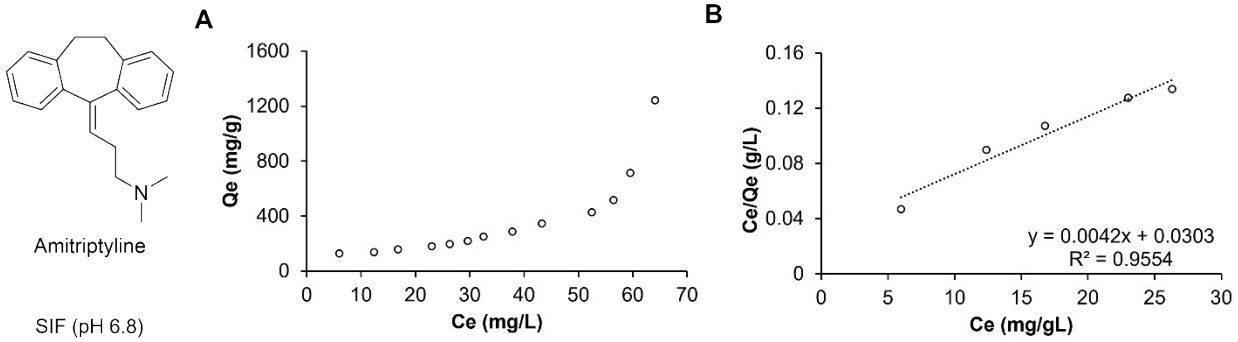

Figure S37. Adsorption isotherm analysis for amitriptyline (AMI) adsorption to E30Y129 in simulated intestinal fluid (SIF, pH 6.8). A) shows the nonlinear adsorption isotherm plotted as equilibrium adsorption capacity (Q_e) versus equilibrium concentration (C_e). B) shows the linearized Langmuir fit applied to the low C_e region to derive apparent maximum adsorption capacity (Q_{max}) and apparent binding affinity (K_L). The fitted parameters are used as comparative descriptors for the low concentration adsorption regime and do not capture non ideal adsorption behavior observed at higher C_e values.

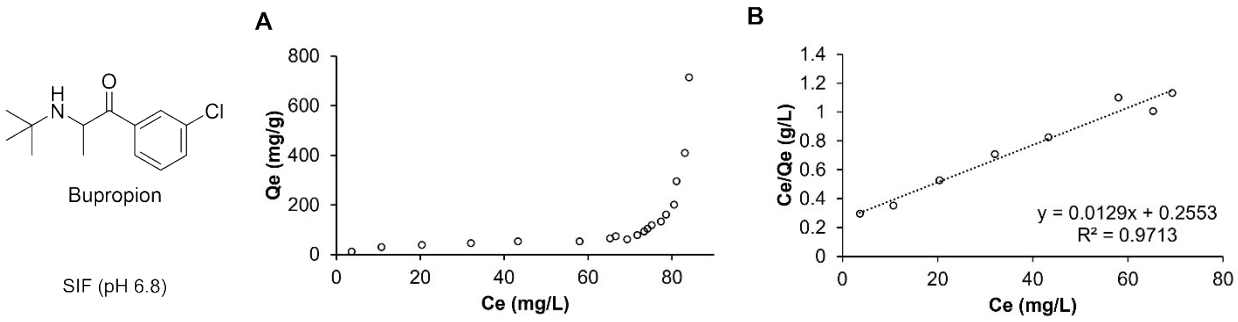

Figure S38. Adsorption isotherm analysis for bupropion (BUP) adsorption to E30Y129 in simulated intestinal fluid (SIF, pH 6.8). A) shows the nonlinear adsorption isotherm plotted as equilibrium adsorption capacity (Q_e) versus equilibrium concentration (C_e). B) shows the linearized Langmuir fit applied to the low C_e region to derive apparent maximum adsorption capacity (Q_{max}) and apparent binding affinity (K_L). The fitted parameters are used as comparative descriptors for the low concentration adsorption regime and do not capture non ideal adsorption behavior observed at higher C_e values.

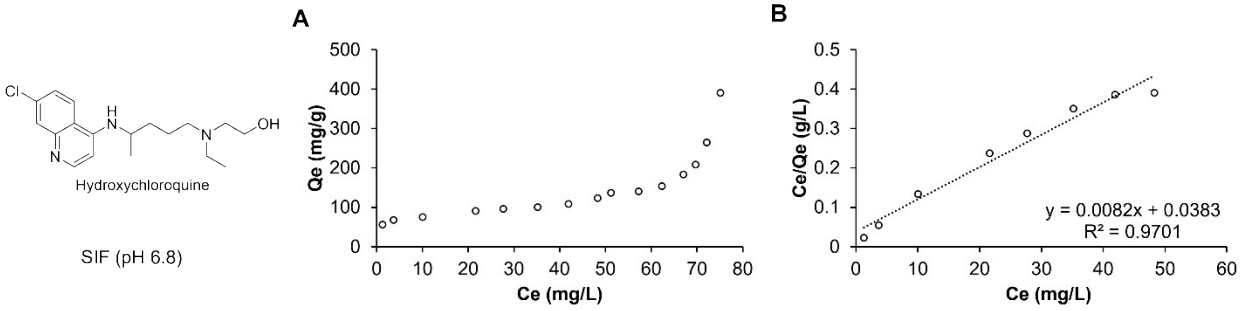

Figure S39. Adsorption isotherm analysis for hydroxychloroquine (HCQ) adsorption to E30Y129 in simulated intestinal fluid (SIF, pH 6.8). A) shows the nonlinear adsorption isotherm plotted as equilibrium adsorption capacity (Q_e) versus equilibrium concentration (C_e). B) shows the linearized Langmuir fit applied to the low C_e region to derive apparent maximum adsorption capacity (Q_{max}) and apparent binding affinity (K_L). The fitted parameters are used as comparative descriptors for the low concentration adsorption regime and do not capture non ideal adsorption behavior observed at higher C_e values.

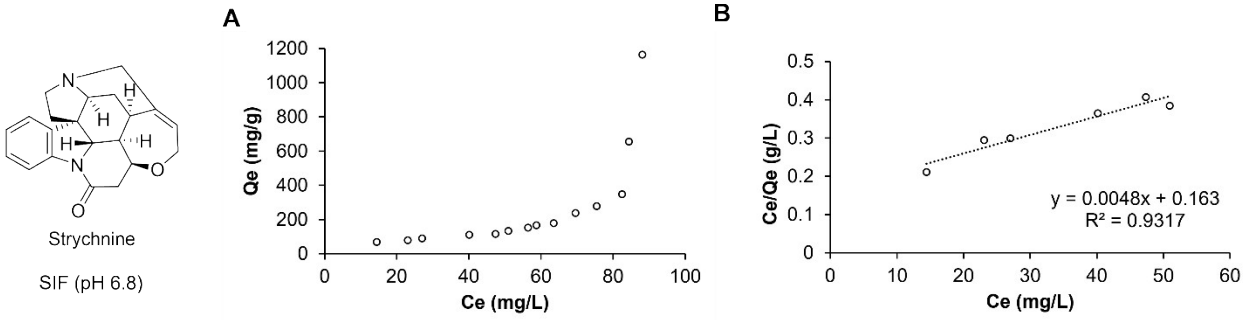

Figure S40. Adsorption isotherm analysis for strychnine (STR) adsorption to E30Y129 in simulated intestinal fluid (SIF, pH 6.8). A) shows the nonlinear adsorption isotherm plotted as equilibrium adsorption capacity (Q_e) versus equilibrium concentration (C_e). B) shows the linearized Langmuir fit applied to the low C_e region to derive apparent maximum adsorption capacity (Q_{max}) and apparent binding affinity (K_L). The fitted parameters are used as comparative descriptors for the low concentration adsorption regime and do not capture non ideal adsorption behavior observed at higher C_e values.

Table S1. Apparent maximum adsorption capacities (Q_{max}) for amitriptyline (AMI), bupropion (BUP), hydroxychloroquine (HCQ), and strychnine (STR) adsorption to E30Y129 and activated charcoal (AC) in simulated gastric fluid (SGF, pH 1.2) and simulated intestinal fluid (SIF, pH 6.8).

Drug	E30Y129 SGF (pH 1.2)	AC SGF (pH 1.2)	E30Y129 SIF (pH 6.8)	AC SIF (pH 6.8)
AMI	161.3 mg/g	175.1 mg/g	238.1 mg/g	492.6 mg/g
BUP	40.5 mg/g	150.9 mg/g	77.5 mg/g	318.6 mg/g
HCQ	50.0 mg/g	224.0 mg/g	122.0 mg/g	264.2 mg/g
STR	58.8 mg/g	197.3 mg/g	208.3 mg/g	234.6 mg/g

E30Y129 values were derived from linearized Langmuir fitting of the low C_e region and are reported as apparent comparative adsorption capacities rather than absolute saturation capacities for the full adsorption process. AC values are included as reference benchmarks from prior adsorption studies. AC reference data included in this table were reported in our prior publications:

1. Wood, H. B.; Trickett, S. M.; Dosch, J. T.; Cao, D. J.; Sydlik, S. A. Adsorption of Antidepressant and Cardiovascular Drugs to Activated Charcoal: Amitriptyline, Bupropion, Minoxidil, Propranolol, and Venlafaxine. *Clinical Toxicology* **2025**, *63* (9), 666–674. DOI: 10.1080/15563650.2025.2532625.
2. Wood, H. B.; Dosch, J. T.; Trickett, S. M.; Cao, D. J.; Sydlik, S. A. Adsorption of Colchicine, Hydroxychloroquine, Ibuprofen, and Strychnine to Activated Charcoal. *Clinical Toxicology* **2026**. DOI: 10.1080/15563650.2026.2615838

Table S2. Apparent binding affinities (K_L) for amitriptyline (AMI), bupropion (BUP), hydroxychloroquine (HCQ), and strychnine (STR) adsorption to E30Y129 and activated charcoal (AC) in simulated gastric fluid (SGF, pH 1.2) and simulated intestinal fluid (SIF, pH 6.8).

Drug	E30Y129 SGF (pH 1.2)	AC SGF (pH 1.2)	E30Y129 SIF (pH 6.8)	AC SIF (pH 6.8)
AMI	0.0172	1.02	0.1386	5.31
BUP	0.0583	0.23	0.0505	0.17
HCQ	0.0210	0.07	0.2141	0.29
STR	0.0075	0.07	0.0294	0.22

E30Y129 values were derived from linearized Langmuir fitting of the low C_e region and are reported as apparent comparative binding affinities rather than global binding constants for the full adsorption process. AC values are included as reference benchmarks from prior adsorption studies. AC reference data included in this table were reported in our prior publications:

1. Wood, H. B.; Trickett, S. M.; Dosch, J. T.; Cao, D. J.; Sydlik, S. A. Adsorption of Antidepressant and Cardiovascular Drugs to Activated Charcoal: Amitriptyline, Bupropion, Minoxidil, Propranolol, and Venlafaxine. *Clinical Toxicology* **2025**, *63* (9), 666–674. DOI: 10.1080/15563650.2025.2532625.
2. Wood, H. B.; Dosch, J. T.; Trickett, S. M.; Cao, D. J.; Sydlik, S. A. Adsorption of Colchicine, Hydroxychloroquine, Ibuprofen, and Strychnine to Activated Charcoal. *Clinical Toxicology* **2026**. DOI: 10.1080/15563650.2026.2615838

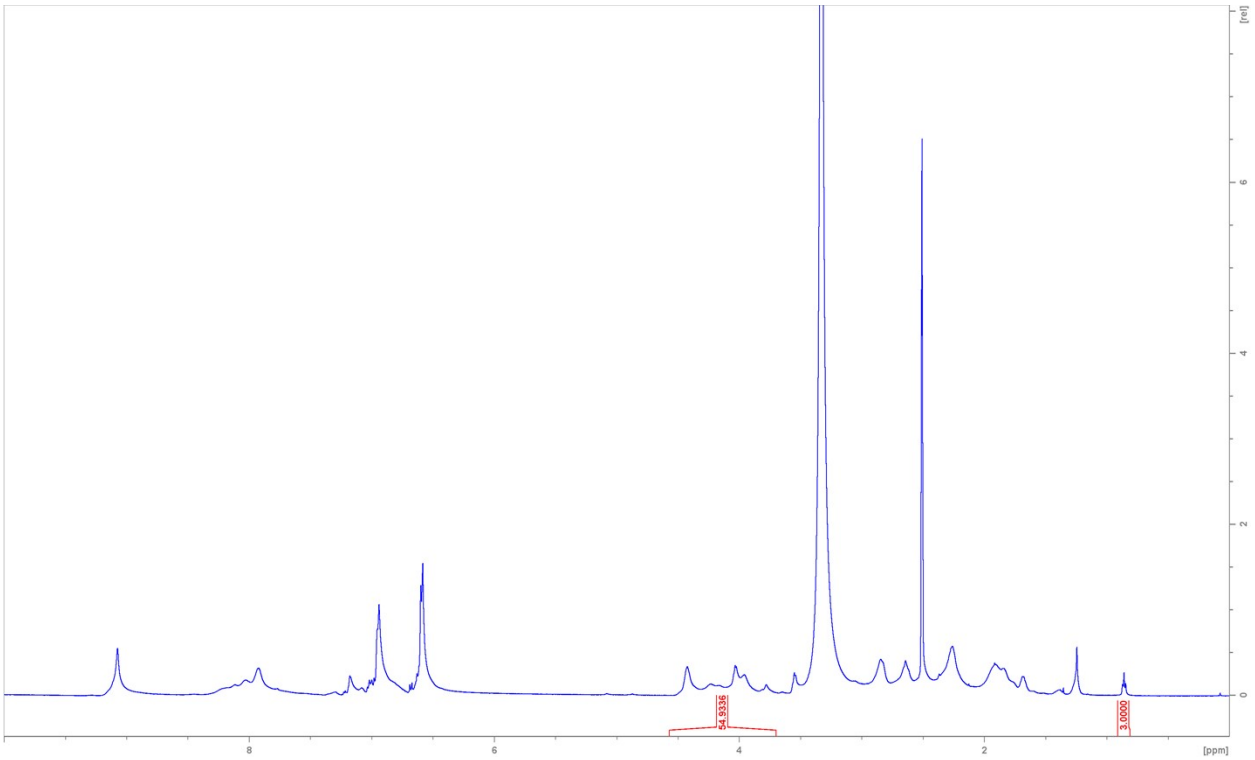

Figure S41. Proton nuclear magnetic resonance (^{1}H NMR) spectrum of E30Y28 in DMSO-d_6 following exposure to simulated gastric fluid (SGF, pH 1.2) containing pepsin for 72 hours at 37 °C. The spectrum and integrals are calibrated to the hexylamine methyl end group at ~0.83 ppm. End group analysis was performed by comparing the peptide backbone proton integrals to the hexylamine methyl end group. Relative to the starting polymer, the reduced peptide backbone integral corresponds to a decrease in number-average repeat units from 58 to 55, consistent with modest degradation under exposure to pepsin in SGF.

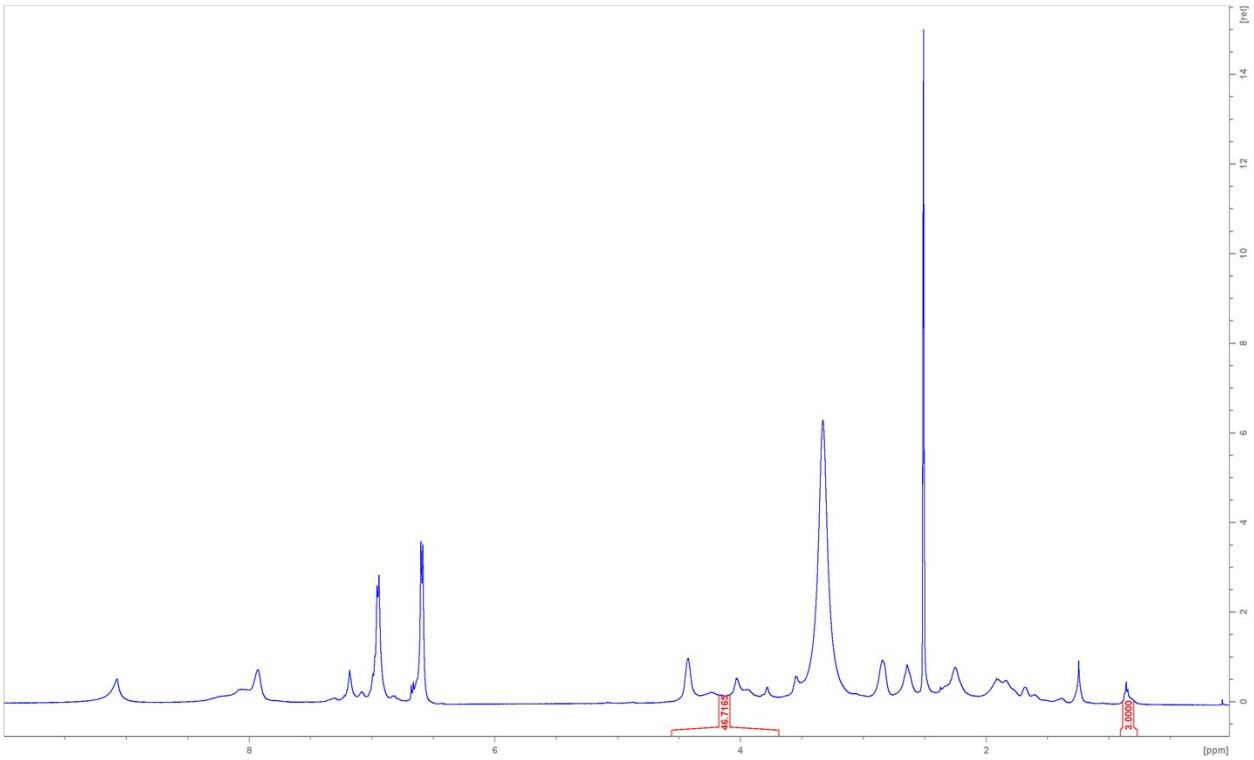

Figure S42. Proton nuclear magnetic resonance (^{1}H NMR) spectrum of E30Y28 in DMSO-d_6 following exposure to simulated intestinal fluid (SIF, pH 6.8) containing trypsin and α-chymotrypsin for 72 hours at 37 °C. The spectrum and integrals are calibrated to the hexylamine methyl end group at ~0.83 ppm. End group analysis was performed by comparing the peptide backbone proton integrals to the hexylamine methyl end group. Relative to the starting polymer, the reduced peptide backbone integral corresponds to a decrease in number-average repeat units from 58 to 47, consistent with greater degradation under exposure to SIF with trypsin and α-chymotrypsin.